HHS Public Access

Author manuscript

Nat Immunol. Author manuscript; available in PMC 2024 October 01.

Published in final edited form as:

Nat Immunol. 2023 October ; 24(10): 1748–1761. doi:10.1038/s41590-023-01589-9.

Identification of human exT$_{reg}$ cells as CD16^{+}CD56^{+} cytotoxic CD4^{+} T cells

Antoine Freuchet[1,5], **Payel Roy**[1,5], **Sujit Silas Armstrong**[1], **Mohammad Oliaeimotlagh**[2], **Sunil Kumar**[2], **Marco Orecchioni**[1,2], **Amal J. Ali**[1], **Amir Khan**[2], **Jeffrey Makings**[1], **Qingkang Lyu**[2], **Holger Winkels**[3,4], **Erpei Wang**[1], **Christopher Durant**[1], **Yanal Ghosheh**[1], **Rishab Gulati**[1], **Felix Nettersheim**[1], **Klaus Ley**[1,2]

[1]La Jolla Institute for Immunology, La Jolla, CA, USA.

[2]Immunology Center of Georgia, Augusta University, Augusta, GA, USA.

[3]University of Cologne, Faculty of Medicine and University Hospital Cologne, Clinic III for Internal Medicine, Cologne, Germany.

[4]Center for Molecular Medicine Cologne (CMMC), University of Cologne, Cologne, Germany.

[5]These authors contributed equally: Antoine Freuchet, Payel Roy.

Abstract

In atherosclerosis, some regulatory T (T$_{reg}$) cells become exT$_{reg}$ cells. We crossed inducible T$_{reg}$ and exT$_{reg}$ cell lineage-tracker mice (*FoxP3*$^{eGFP-Cre-ERT2}$ *ROSA26*$^{CAG-fl-stop-fl-tdTomato}$) to atherosclerosis-prone *Apoe*$^{-/-}$ mice, sorted T$_{reg}$ cells and exT$_{reg}$ cells and determined their transcriptomes by bulk RNA sequencing (RNA-seq). Genes that were differentially expressed between mouse T$_{reg}$ cells and exT$_{reg}$ cells and filtered for their presence in a human single-cell RNA-sequencing (scRNA-seq) panel identified exT$_{reg}$ cell signature genes as *CST7, NKG7,*

Correspondence and requests for materials should be addressed to Klaus Ley. kley@augusta.edu.

Author contributions

K.L., A.F., P.R. and S.S.A. designed the experimental and analytical workflow. A.F. and P.R. conducted most experiments, analyzed and assembled data and drafted parts of the paper. S.S.A., M.O., A.K., J.M., Y.G. and R.G. conducted bioinformatic data analysis. S.K. conducted flow cytometry. M. Orecchioni conducted RT–qPCR and mouse proliferation experiments. A.J.A. and H.W. generated the mouse strain by breeding. A.J.A. generated most of the mouse data. Q.L. assisted in data analysis. E.W. prepared libraries for human bulk RNA-seq experiments. C.D. prepared human single-cell and mouse bulk RNA-seq libraries. F.N. assisted in mouse strain maintenance and provided expertise in proliferation experiments. K.L. conceived and supervised the study, provided funding and wrote the paper. We acknowledge the support from funding agencies. Our work is supported by the National Institutes of Health awards P01 HL136275 and R35 HL145241 to K.L., the American Heart Association's Career Development Award (941152) to M. Orecchioni, a fellowship from Neven-DuMont Foundation to H.W. and a Deutsche Forschungsgemeinschaft fellowship (NE 2574/1–1) to F.N.

Code availability

No new algorithms were generated for this study.

Competing interests

The authors declare no competing interests.

Additional information

Extended data is available for this paper at https://doi.org/10.1038/s41590-023-01589-9.

Supplementary information The online version contains supplementary material available at https://doi.org/10.1038/s41590-023-01589-9.

Peer review information *Nature Immunology* thanks the anonymous reviewers for their contribution to the peer review of this work. Primary Handling Editor: L. A. Dempsey, in collaboration with the *Nature Immunology* team. Peer reviewer reports are available.

GZMA, *PRF1*, *TBX21* and *CCL4*. Projecting these genes onto the human scRNA-seq with CITE-seq data identified human exT_{reg} cells as $CD3^+CD4^+CD16^+CD56^+$, which was validated by flow cytometry. Bulk RNA-seq of sorted human exT_{reg} cells identified them as inflammatory and cytotoxic $CD4^+$T cells that were significantly distinct from both natural killer and T_{reg} cells. DNA sequencing for T cell receptor-β showed clonal expansion of T_{reg} cell CDR3 sequences in exT_{reg} cells. Cytotoxicity was functionally demonstrated in cell killing and CD107a degranulation assays, which identifies human exT_{reg} cells as cytotoxic $CD4^+$T cells.

Atherosclerosis is a chronic inflammatory disease of the artery walls with clear evidence of a systemic $CD4^+$T cell-mediated autoimmune response to apolipoprotein B (ApoB) epitopes in mice[1–5] and humans[3,6,7]. T_{reg} cells play a protective role via anti-inflammatory cytokines and contact-dependent mechanisms[8,9] and represent a promising therapeutic tool. Under inflammatory conditions, T_{reg} cells become plastic, that is, they acquire lineage-defining transcription factors in addition to FoxP3 (called T_H-like T_{reg} cells)[10–12], like T-bet for T_H1 or RORγt for T_H17. In chronic inflammation, T_{reg} cells become unstable and lose CD25 and FoxP3 expression[13]. Such exT_{reg} cells have been identified in mouse disease models such as in type 1 diabetes[14], experimentally induced autoimmune encephalomyelitis[15], arthritis[16] and atherosclerosis[4,7,10,11,17]. In some studies, exT_{reg} cells have been reported to express RORγT and produce interleukin (IL)-17A[14,16,18], or T-bet and interferon (IFN)-γ[14,15,19] or Bcl6 and CXCR5 (ref. 17). However, complete transcriptomes of exT_{reg} cells have not been reported. Here, we use the inducible T_{reg} cell lineage-tracker mouse strain *FoxP3-eGFP*$^-$*Cre-ERT2* (ref. 20) *ROSA26CAG-fl-stop-fl-tdTomato*, crossed into atherosclerosis-prone *Apoe*$^{-/-}$ mice. Tamoxifen injection induces the generation of tdTomato and GFP-expressing $Foxp3^+$ T_{reg} cells. Converted exT_{reg} cells are detectable as $GFP^-tdTomato^+CD4^+$T cells.

Human exT_{reg} cells are suspected to exist, but have not been described. In a previous study, transcriptomic analysis of tetramer-sorted APOB-specific human $CD4^+$ T cells, which are expected to contain T_{reg} cells and exT_{reg} cells based on the mouse studies[4,7,11,17], revealed that exT_{reg} cells are not similar to T_{reg} cells[7]. In fact, exT_{reg} cells mapped widely across a uniform manifold approximation and projection (UMAP) plot constructed of T_{reg} cells, T_H1 and memory T cells. The present study was designed to identify human exT_{reg} cells by using an integrated approach of mapping gene signatures from sorted mouse exT_{reg} cell transcriptomes to human scRNA-seq with cellular indexing of transcriptomes and epitopes sequencing (CITE-seq) data, followed by T cell antigen receptor sequencing (TCR-seq), bulk RNA-seq and functional characterization of sorted human exT_{reg} cells. Bulk RNA-seq of sorted T_{reg} cells and exT_{reg} cells from the lineage-tracker mice on the *Apoe*$^{-/-}$ background yielded high-quality transcriptomes identifying hundreds of differentially expressed genes (DEGs). Then, we extracted gene signatures from exT_{reg} cells and mapped them to a published and publicly available human peripheral blood mononuclear cell (hPBMC) scRNA-seq dataset[21]. This dataset also had information on cell surface phenotype by CITE-seq. This identified surface markers on $CD4^+$T cells that expressed the exT_{reg} cell signature genes. These were in turn used to sort the putative exT_{reg} cells from human blood, obtain high-quality, deep transcriptomes and assess their function. To identify the provenance of human exT_{reg} cells, we used TCRβ sequencing. We reasoned that exT_{reg}

cells derived from T_{reg} cells might show clonal expansion of TCRβ sequences found in T_{reg} cells. TCR diversity was assessed by analyzing TCR CDR3 sequences directly and using GLIPH[22].

Results

Differentially expressed mouse exT_{reg} and T_{reg} cell-classifying genes

To track exT_{reg} cells in mice under conditions of chronic sterile inflammation, we used a recently published mouse model[7], in which we crossed an inducible *FoxP3*-Cre lineage-tracker mouse strain (*FoxP3*$^{eGFP\text{-}Cre\text{-}ERT2}$*ROSA26*$^{CAG\text{-}fl\text{-}stop\text{-}fl\text{-}tdTomato}$) into the atherosclerosis-prone *Apoe*$^{-/-}$ mouse strain. Both strains are in a C57BL/6 background. *Apoe*$^{-/-}$ mice develop atherosclerosis with chronic inflammation, which can trigger T_{reg} cell instability and exT_{reg} cell formation. In tamoxifen-injected mice, $GFP^+tdTomato^+$ T_{reg} cells and $GFP^-tdTomato^+$ exT_{reg} cells are detected as distinct $CD4^+$T cell subsets, with negligible GFP^+ or $tdTomato^+$ cells among control non-T cells and $CD4^-$ T cells (Extended Data Fig. 1a). We quantified the frequencies of T_{reg} cells ($GFP^+tdTomato^+$) and exT_{reg} cells ($GFP^-tdTomato^+$) in the spleen and lymph nodes (LNs) of these mice at 4, 8, 12 and 20 weeks of age after tamoxifen injection (Fig. 1a). At 4 weeks, exT_{reg} cells accounted for <1% of total $CD4^+$T cells in either organ. They gradually accumulated over time, reaching ~7% in spleen and ~4% in LNs at 20 weeks. As previously reported[10,14], we observed significantly lower surface expression of CD25 in exT_{reg} cells (Fig. 1b) than in T_{reg} cells.

Mice of both sexes were maintained on a regular chow diet (CD) and LNs and spleens were collected at 20 weeks after tamoxifen injection. T_{reg} cells ($TCR\beta^+CD4^+GFP^+tdTomato^+$) and exT_{reg} cells ($TCR\beta^+C\ D4^+GFP^-tdTomato^+$) were sorted by flow cytometry (sorting scheme as previously described[7]) and sequenced using an optimized bulk RNA-seq method. In the principal component analysis (PCA), principal component (PC) 1 distinguished between T_{reg} cells and exT_{reg} cells and PC2 distinguished between the site of origin (LNs or spleens; Fig. 1c). The first two components explained the majority (86%) of the transcriptome variance. The mouse genes were filtered for human orthologs and intersected with a published dataset of 496 human genes that were analyzed by scRNA-seq with CITE-seq[21]. Mouse orthologs were found for 383 of the 496 human genes (Supplementary Table 1). Expression of these 383 genes in the transcriptomes from sorted mouse T_{reg} cells and exT_{reg} cells were used to train a support vector machine (SVM) model. T_{reg} cell versus exT_{reg} cell genes were ranked by weight and the top 60 classifying genes were identified for each subset (Supplementary Table 2). As expected, the top 60 genes classifying T_{reg} cells included *Foxp3* and *Il2ra* (encoding CD25; Extended Data Fig. 1b). The top 60 genes classifying exT_{reg} cells included *Tbx21, Gzmk, Prf1, Nkg7, Ifng* and *Ccl4* (Extended Data Fig. 1b). Most (50 of 60 T_{reg} cell genes and 51 of 60 exT_{reg} cell genes) were significantly (P adjusted < 0.05) differentially expressed between mouse T_{reg} cells and exT_{reg} cells (Fig. 1d, statistics in Supplementary Table 3). T_{reg} cells and exT_{reg} cells were also found in the artery wall (Fig. 1e), but numbers were insufficient for cell sorting.

exT$_{reg}$ cell-specific genes and surface markers in human CD4$^+$ T cells

Mouse exT$_{reg}$ DEGs (Fig. 1d, up in exT$_{reg}$ cells) were projected onto the UMAP projections of a published scRNA-seq transcriptome and CITE-seq dataset from 40,821 CD4$^+$ T cells from 61 participants in the Coronary Assessment in Virginia (CAVA) cohort[21]. This cohort contains men and women, aged from 40 to 80 years, with coronary artery disease (CAD) quantified by angiography (Gensini scores), where Gensini scores <6 were considered CAD$^-$ and scores >30 were considered CAD$^+$. A full description of the cohort is published[21]. Statistical significance ($P < 0.05$) of exT$_{reg}$ cell gene enrichment (pct.1 and $\log_2$ fold change) in each CD4$^+$ T cell cluster versus the other CD4$^+$ T clusters, (one-versus-all) was evaluated. Six genes (*CST7*, *NKG7*, *GZMA*, *PRF1*, *TBX21*, *CCL4*) showed high and specific expression in cluster CD4T_7 (encompassing 1,359 cells), which was previously classified as cytotoxic effector memory cells[21] (Fig. 2a). In the UMAP projections of human CD4$^+$ T cells, each of the six exT$_{reg}$ cell classifier genes was most highly expressed in cells that mapped to CD4T_7 (Extended Data Fig. 2a). The *FOXP3*-expressing T$_{reg}$ cells resided in cluster CD4T_17, which was previously identified as the T$_{reg}$ cluster[21] (Fig. 2b). The fraction of cells expressing the exT$_{reg}$ candidate genes was significantly higher in cluster 7 than in T$_{reg}$ cells for all six genes (Fig. 2c).

Having learned that cluster 7 likely contains human exT$_{reg}$ cells, we wished to deconvolve their identities at single-cell resolution. Serial combinations of the six candidate exT$_{reg}$ markers improved specificity and identified consecutively smaller CD4$^+$ T cell populations (Supplementary Table 4). Coexpression of *CST7* and *NKG7* was found in 9.4% of all CD4$^+$ T cells; coexpression of *CST7* and *GZMA* in 8.7%; *CST7*, *NKG7* and *GZMA* in 7.1%; *CST7*, *NKG7*, *GZMA* and *PRF1* in 3.5%; *CST7*, *NKG7*, *GZMA*, *PRF1* and *TBX21* in 1.1% (candidate 5 in Fig. 2d) and *CST7*, *NKG7*, *GZMA*, *PRF1*, *TBX21* and *CCL4* in 0.3% (candidates 1–4 and 6 in Extended Data Fig. 2b).

We considered exT$_{reg}$ cell candidate 5 (Fig. 2d) optimal, because this signature identified no cells in the T$_{reg}$ cell cluster CD4T_17 and showed negligible expression in other CD4$^+$ T cell clusters.

Next, we studied the cell surface phenotype of the candidate human exT$_{reg}$ cells, based on the CITE-seq data (51 antibodies). Analysis of differentially expressed surface markers on candidate exT$_{reg}$ cells versus T$_{reg}$ cells (Fig. 2e) revealed statistically significant ($P < 0.05$) overexpression of CD16, CD56 and CD127 (Fig. 2e). Projecting CD56 and CD16 surface expression onto the UMAP revealed that CD56 protein was expressed on the surface of 1,681 cells (4.1% of all CD4$^+$ T cells; Extended Data Fig. 2c). CD16 was expressed on fewer cells (109 cells, 0.3% of all CD4$^+$ T cells; Extended Data Fig. 2c). Interestingly, almost all CD16$^+$ cells coexpressed CD56 (94 of 109 cells; Fig. 2f). This analysis thus identified two markers by which candidate human exT$_{reg}$ cells could be sorted: CD56 and CD16.

Having identified CD56 and CD16 as surface markers for candidate human exT$_{reg}$ cells, we conducted flow cytometry on PBMCs and found that some CD4$^+$T cells coexpressed CD16 and CD56 protein on their surface (Fig. 2g, with fluorescence-minus-one (FMO) controls; more gating strategy in Extended Data Fig. 2d). T$_{reg}$ cells were identified as

$CD25^+CD127^{lo}CD4^+$T cells (Fig. 2g, with FMOs). Quantitative analysis by flow cytometry showed that exT_{reg} cells, unlike T_{reg} cells, expressed high levels of CD16, CD56 and CD127, and low levels of FOXP3 protein (Fig. 2h). We sorted $CD16^+CD56^+$ exT_{reg} cells and $CD25^+CD127^{lo}$ T_{reg} cells, prepared cDNA and conducted quantitative PCR with reverse transcription (RT–qPCR) for the six exT_{reg} cell signature genes (*CST7*, *NKG7*, *GZMA*, *PRF1*, *TBX21* and *CCL4*). Normalized transcript expression levels of all these genes were significantly upregulated in exT_{reg} cells compared to T_{reg} cells (Extended Data Fig. 2e).

Deep transcriptomes of human $CD16^+CD56^+$ exT_{reg} cells

Having established that human exT_{reg} cells can be isolated using CD16 and CD56, we next sorted $CD4^+CD16^+CD56^+$ exT_{reg} cells from seven donors and compared their transcriptomes with $CD4^+CD25^+CD127^{lo}$ T_{reg} cells (sorting scheme in Extended Data Fig. 3a). PCA revealed that exT_{reg} cells clustered far from T_{reg} cells (Fig. 3a). PC1 (56% of variance) was the main driver of this separation (Fig. 3a and Supplementary Table 5). Human exT_{reg} cells had lost *FOXP3* and *IL2RA* expression (Fig. 3b). They significantly gained cytotoxic and inflammatory genes like *NKG7*, *TBX21*, *CCL3*, *CCL4* and *CCL5*, all of which were not expressed or present at low levels in T_{reg} cells (Fig. 3b). This pattern of gene expression was also seen in the mouse dataset (Extended Data Fig. 4a).

Gene-set enrichment analysis (GSEA) of human bulk exT_{reg} cell transcriptomes against the human scRNA-seq dataset confirmed their enrichment in CD4 cluster 7 (normalized enrichment score (NES) 1.82, false discovery rate $q = 7.8 \times 10^{-4}$, Extended Data Fig. 3b). Similarly, mouse exT_{reg} genes, filtered for human orthologs in the scRNA-seq panel, positively correlated with human exT_{reg} cell genes from bulk RNA-seq (NES = 1.497, false discovery rate $q = 0.033$, Extended Data Fig. 4b). This formally showed that the leading exT_{reg} cell gene signatures are significant and consistent among the three datasets (mouse bulk RNA-seq, human scRNA-seq, human bulk RNA-seq). Pathway analysis on all genes that were significantly upregulated in human exT_{reg} cells, compared to T_{reg} cells (Supplementary Table 6) revealed significant (adjusted P value < 0.05) enrichment of cellular processes related to TCR, Notch, cytokine and receptor-mediated signaling, metabolism, cytotoxicity, adhesion and hemostasis (Extended Data Fig. 3c).

In humans, CD16 and CD56 are canonical markers of natural killer (NK) cells. Unlike NK cells, human exT_{reg} cells expressed CD3 subunits (Fig. 3c,d). We compared our exT_{reg} cell transcriptomes from both mouse and human bulk RNA-seq datasets with publicly available NK cell data. DEGs were filtered for significance in both species (human in Fig. 3c; mouse in Extended Data Fig. 4c). The TCR-related signaling complex genes *CD3D*, *CD3E* and *CD3G* were all significantly higher in exT_{reg} cells than in NK cells. *TCF7*, encoding a transcription factor involved in T cell development and memory differentiation, was also significantly higher in exT_{reg} cells than in NK cells. *CD27*, known to be absent on mature human NK cells[23], was significantly expressed in ex T_{reg} cells. Conversely, *KLRD1* (encoding CD94) and *FCER1G* were significantly higher in NK cells (Fig. 3c). The identity of $CD3^+CD4^+CD16^+CD56^+$ human exT_{reg} cells and $CD3^-CD4^-CD16^+CD56^+$ human NK cells was also confirmed by fluorescence-activated cell sorting (FACS; representative plots in Fig. 3d; gating scheme in Extended Data Fig. 3d).

exT$_{reg}$ cells, and not NK cells, expressed TCRαβ, CCR7, CD127 and CD27 proteins on the surface (representative histograms in Fig. 3e; quantification in Fig. 3f). Taken together, we found that the exT$_{reg}$ cell gene signatures were conserved between mice and humans. Human CD3$^+$CD4$^+$CD16$^+$CD56$^+$ exT$_{reg}$ cells are distinct from both T$_{reg}$ cells and NK cells.

TCRβ sequencing shows clonal expansion of human exT$_{reg}$ cells from T$_{reg}$ cells

To study the provenance of human CD16$^+$CD56$^+$CD4$^+$T cells, we used TCRB sequencing. We reasoned that if CD16$^+$CD56$^+$ T cells are exT$_{reg}$ cells, their TCRB CDR3 sequences would overlap with TCRB CDR3 sequences in T$_{reg}$ cells. Moreover, if exT$_{reg}$ cells arise by clonal expansion from T$_{reg}$ cells, we expected to see clonal enrichment. Thus, we sequenced TCRβ from sorted T$_{reg}$ cells (CD25^{hi}CD127^{lo}) and exT$_{reg}$ cells (CD16$^+$CD56$^+$) CD4$^+$T cells from four healthy donors (sorting strategy was the same as that used for bulk RNA-seq, Extended Data Fig. 3a; number of templates and rearrangements in Supplementary Table 7). For comparison, we included naïve CD4$^+$T cells (CD45RA$^+$CCR7$^+$). Simpson's clonality was higher in exT$_{reg}$ cells than in T$_{reg}$ cells or naïve CD4$^+$T cells (Fig. 4a). Morisita's index, a measure of overlap between samples, showed a significantly higher frequency of shared rearrangements of exT$_{reg}$ cells with T$_{reg}$ cells than with naive T cells (Fig. 4b).

For a more detailed analysis, we used GLIPH[22], a software that identifies conserved amino acid sequence patterns in CDR3 sequences. First, we filtered the GLIPH groups based on their enrichment (Fisher $P < 0.05$) in our dataset, as compared to a published set of CDR3 sequences from naïve T cells[22]. CDR3 sequence patterns with exT$_{reg}$ TCRs were filtered for statistically significant expansion based on the productive frequencies of their TCRs (expansion score $P < 0.05$). We identified 345 expanded exT$_{reg}$ cell groups. TCRβ sequences from T$_{reg}$ cells were present in ~50% (178 of 345) of them (Supplementary Table 8). We compared the relative abundance of T$_{reg}$ cell and exT$_{reg}$ cell TCRβ sequences in these groups and found many TCRβ CDR3 patterns that were significantly expanded ($\log_2$FC ± 1, Poisson test $P < 0.05$) in exT$_{reg}$ cells compared to T$_{reg}$ cells (Fig. 4c; GLIPH patterns in Supplementary Table 9).

The clonal expansion observed in exT$_{reg}$ cells prompted us to reason that T$_{reg}$ cells may have proliferated and differentiated into oligoclonal exT$_{reg}$ cells. This was supported by our observation that the SVM model had identified genes related to DNA replication and cell cycle, such as *Aurkb*, *Ccnd2*, *Mcm4*, *Mki67* and *Top2a*, as T$_{reg}$ cell-classifying genes (Supplementary Table 2). These genes were significantly upregulated in mouse T$_{reg}$ cells, compared to exT$_{reg}$ cells (Extended Data Fig. 1b and Supplementary Table 3). To functionally compare T$_{reg}$ cell versus exT$_{reg}$ cell proliferation in atherosclerotic mice, we conducted an in vivo BrDU incorporation experiment in *FoxP3*$^{eGFP\text{-}Cre\text{-}ERT2}$ *ROSA26*$^{CAG\text{-}fl\text{-}stop\text{-}fl\text{-}tdTomato}$ *Apoe*$^{-/-}$ mice (experimental design in Extended Data Fig. 5a). Proliferating T$_{reg}$ cells and exT$_{reg}$ cells (gating scheme, controls and representative plots in Extended Data Fig. 5b–d) were monitored based on Ki67 (encoded by *Mki67*) expression and BrDU incorporation. Frequencies of Ki67$^+$BrDU$^+$CD4$^+$T cells were significantly higher among T$_{reg}$ cells than exT$_{reg}$ cells (quantification in Extended Data Fig. 5d), showing that mouse T$_{reg}$ cells actively proliferate during atherosclerosis.

Next, we examined proliferation-related genes in our human bulk RNA-seq dataset (Fig. 3). We found that human T_{reg} cells, as compared to exT_{reg} cells, expressed significantly higher transcript levels of *MKI67* (gene encoding Ki67), topoisomerase *TOP2A*, *MCM2*, *MCM3*, *MCM5* and *MCM6* (members of the replicative helicase that are involved in the formation of pre-replicative complexes) and cyclin A and B genes (which activate DNA replication and mitosis, respectively; Fig. 4d). These data are consistent with the idea that exT_{reg} cells may arise from T_{reg} cells by proliferation and clonal expansion.

To assess whether human exT_{reg} cells retain any phenotypic similarities with T_{reg} cells, we monitored expression of the T_{reg} cell markers PD-1, GITR, LAG3 and TIGIT on exT_{reg} cells using FACS (representative plots and FMO controls in Extended Data Fig. 6, quantification in Fig. 4e). All $CD4^+$T cells were used as a negative control. exT_{reg} cells retained TIGIT and GITR, expressed significantly more PD-1 than T_{reg} cells, and gained expression of LAG3. We also filtered the transcriptomes of human exT_{reg} cells by known T_{reg} genes[24] and found 32 such genes that were retained in exT_{reg} cells (Supplementary Table 10).

Human exT_{reg} cells are not suppressive but cytotoxic

To test whether human exT_{reg} cells retained the suppressive capacity of T_{reg} cells, we conducted a suppression assay to compare the effects of T_{reg} cells and exT_{reg} cells on the proliferation of effector T cells (T_{eff}) cells. Co-culturing T_{reg} cells with T_{eff} cells at a 1:1 T_{reg}:T_{eff} cell ratio effectively suppressed proliferation of T_{eff} cells, as measured by carboxyfluorescein succinimidyl ester (CFSE) dilution (Fig. 5a). By contrast, T_{eff} cell proliferation in the presence of exT_{reg} cells (Fig. 5a) remained the same as proliferation of T_{eff} cells alone (Fig. 5a). T_{eff} cell proliferation was significantly higher when co-cultured with exT_{reg} cells than with T_{reg} cells (Fig. 5a) and not different from proliferation of T_{eff} cells alone.

To delineate the functional profile of human exT_{reg} cells, we carefully examined their transcriptomes (Fig. 3) and contrasted them with T_{reg} cells (heat map of DEGs in Fig. 5b). We found that human exT_{reg} cells expressed many genes present in the KEGG list of cytotoxic genes. These included *GZMB*, *PRF1* and *FASLG*, known to mediate effector functions in cytotoxic cells. Additionally, exT_{reg} cells had lost *FOXP3*, *IL2RA*, *CTLA4*, *IL10* and *LRRC32* gene expression, supporting their functional loss of suppressive capacity.

We validated intracellular expression of perforin (encoded by *PRF1*), granzyme B (encoded by *GZMB*) and FAS ligand (encoded by *FASLG*) in human exT_{reg} cells at the protein level by FACS. We detected high expression of perforin and granzyme B, but not FAS ligand on exT_{reg} cells (representative histograms in Fig. 5c; quantification in Fig. 5c). Although both exT_{reg} cells and NK cells expressed the cytotoxic marker perforin, only exT_{reg} cells upregulated the activation-induced $CD4^+$T cell marker CD40L, upon stimulation with phorbol 12-myristate 13-acetate (PMA) and ionomycin (Extended Data Fig. 7). In a degranulation assay with P815 target cells, crosslinking with anti-CD3 triggered surface mobilization of the degranulation marker CD107a specifically in exT_{reg} cells and not in NK cells (representative histograms in Fig. 5d, quantification in Fig. 5d). These functional data further confirm that exT_{reg} cells are distinct from NK cells. To directly test the cytotoxic potential of exT_{reg} cells, we used anti-CD3-coated P815 target cells and co-cultured

them with sorted human exT_{reg} cells at a 1:5 target-to-effector ratio. $CD8^+$ cytotoxic T lymphocytes (CTLs) were used as positive control. T_{reg} cells were used as a negative control. exT_{reg} cells showed cytotoxicity in the same range as bona fide $CD8^+$ CTLs (Fig. 5e). As expected, T_{reg} cells showed no cytotoxicity (Fig. 5e).

These data collectively show that $CD16^+CD56^+$ exT_{reg} cells do not exhibit T_{reg} cell-like suppressive properties and instead acquire cytotoxicity, although they retain some T_{reg} cell genes and markers. Unlike cytotoxic NK cells, exT_{reg} cells can be activated by TCR-related stimulation and express T cell markers upon activation.

Human exT_{reg} cells express cytotoxic and inflammatory markers

We recently reported that mouse exT_{reg} cells, unlike T_{reg} cells, express tumor necrosis factor (TNF) and IFN-γ[7]. Here we compared the expression of cytotoxic and inflammatory cytokines in human T_{reg} cells and exT_{reg} cells in an intracellular cytokine staining (ICS) assay (gating scheme in Extended Data Fig. 8a). About 60% of exT_{reg} cells coexpressed granzyme B and perforin (Fig. 6a). We confirmed that about 30–40% of exT_{reg} cells expressed intracellular TNF protein as measured by flow cytometry (Fig. 6a). Basal expression of IFN-γ was low in unstimulated exT_{reg} cells but strongly upregulated upon activation with PMA and ionomycin (Fig. 6b). Stimulation-induced IFN-γ production was significantly higher in exT_{reg} cells than in T_{reg} cells (Fig. 6b).

In our gene expression analysis (Fig. 3b), the chemokines *CCL3*, *CCL4* and *CCL5* were significantly higher in human exT_{reg} cells than in T_{reg} cells. Using FACS, we confirmed that intracellular protein expression of all three chemokines was specifically enriched in exT_{reg} cells and not detected in bulk $CD4^+$T cells (Fig. 6c). About 60% of exT_{reg} cells expressed CCL3 or CCL4 proteins (Fig. 6c). CCL5 expression was found in 70–80% of exT_{reg} cells (Fig. 6c). These chemokines attract monocytes[25] and promote inflammation.

Chemokine receptors play a major role in T cell trafficking and tissue infiltration. In the pathway analysis of human exT_{reg} genes, the CXCR4 signaling pathway was significantly enriched (Extended Data Fig. 3c). To confirm this finding, we used flow cytometry to monitor the expression of CXCR4 and other inflammation-related chemokine receptors such as CCR5, CXCR2, CXCR3 and CX3CR1. Expression of all these receptors was significantly higher on ex T_{reg} cells than on bulk $CD4^+$T cells (representative data and FMO controls in Extended Data Fig. 8b, quantification in Fig. 6d). About 20% of exT_{reg} cells expressed CCR5 or CXCR2. CXCR3, CXCR4 and CX3CR1 could be detected in about 50–60% of exT_{reg} cells. In atherosclerotic mice, CCR5 expression on T cells is required for T cell homing to aortic lesions[10]. CXCR3 is a well-established inflammatory chemokine receptor expressed on T_H1 cells and on activated effector and memory T cells that migrate to inflammatory lesions[26]. CXCR2 was highly expressed on $CD4^+$T cells that infiltrated gray matter tissue in a mouse model of multiple sclerosis[27]. CX3CR1 has been shown to be expressed on highly polarized cytotoxic dengue-virus specific $CD4^+$T cells in humans[28]. Its ligand CX3CL1 is highly expressed in atherosclerotic lesions[29,30]. SDF-1, the ligand for CXCR4, has been detected at higher levels in human atherosclerotic plaques, and not in normal blood vessels[31].

Inflammatory and cytotoxic genes in exT_{reg} cells from individuals with coronary artery disease

The CAVA cohort, from which the scRNA-seq data with CITE-seq came, encompasses participants with Gensini scores > 30 (CAD^+) and < 6 (CAD^-). First, we intersected the genes significantly upregulated in human exT_{reg} cells (up in exT_{reg} cells; Supplementary Table 6) with the genes tested in the human scRNA-seq dataset and found 108 such genes (Fig. 7a and Supplementary Table 11). Next, we tested which of these genes were expressed at significantly higher levels in exT_{reg} cells from CAD^+ cases as compared to CAD^- controls. In non-diabetic CAD^+ individuals, we found that *CNOT2*, *CCL4*, *IL18RAP*, *KLRG1*, *KLRC1*, *LYN*, *SAMD3* and *SYNE1* were significantly upregulated (Fig. 7b) compared to CAD^- controls (Fig. 7b). In exT_{reg} cells from diabetic individuals with CAD (Fig. 7b), *CCL5*, *FGFBP2*, *ITGA4*, *ITGAM*, *KLRB1* and *KLRC1* were significantly higher in CAD^+ than in CAD^- individuals (Fig. 7b). *KLRC1* was found to be significantly overexpressed in both non-diabetic and diabetic CAD^+ individuals. Statistical analysis of the differential expression of these 13 genes between exT_{reg} cells and T_{reg} cells showed highly significant upregulation in human ex T_{reg} cells (Fig. 7c).

In summary, using gene signatures from mouse exT_{reg} cells, we identified human $CD3^+CD4^+CD16^+CD56^+$ T cells as human exT_{reg} cells and validated expression of exT_{reg} signature genes and surface markers. Bulk RNA-seq showed that exT_{reg} cells are very different from T_{reg} cells and NK cells, representing a distinct subset of $CD4^+$T cells. Human exT_{reg} cells express inflammatory and cytotoxic genes and retain some T_{reg} cell markers. TCR-seq showed shared T_{reg}/exT_{reg} cell TCRB clones that were more expanded in exT_{reg} cells compared to T_{reg} cells. Such oligoclonal exT_{reg} cells likely originated from proliferating T_{reg} cells. Functionally, human exT_{reg} cells lack suppressive capacity and have acquired cytotoxic properties. They express cytotoxic effectors, inflammatory cytokines, chemokines and chemokine receptors. Expression of multiple inflammatory and cytotoxic genes in exT_{reg} cells is augmented in individuals with CAD compared to CAD^- controls.

Discussion

Our findings define human exT_{reg} cells as $CD3^+CD4^+CD56^+CD16^+$ T cells. These cells express the exT_{reg} signature genes *CST7, NKG7, GZMA, PRF1, TBX21* and *CCL4*. At the protein level, human exT_{reg} cells express T cell markers like TCRαβ, CCR7, CD27 and CD127. Inflammatory chemokine receptors including CCR5, CXCR2, CXCR3, CXCR4 and CX3CR1 were enriched on exT_{reg} cells. Most human exT_{reg} cells also expressed granzyme B and the monocyte-attracting, pro-inflammatory chemokines CCL3, CCL4 and CCL5. They upregulated IFN-γ production upon stimulation. Unlike T_{reg} cells, exT_{reg} cells expressed little FOXP3 and completely failed to suppress T_{eff} cell proliferation. Instead, they exerted cytotoxic effects. Clonality analysis by TCRβ sequencing revealed that exT_{reg} cells contain expanded clones sharing TCR CDR3 sequences with T_{reg} cells.

It is estimated that 80% of systemic T_{reg} cells come from the thymus (tT_{reg} cells)[32,33]. The remaining 20% are induced from conventional T cells in the periphery (iT_{reg} cells). Both nT_{reg} cells and iT_{reg} cells are mostly in LNs, but some are found in the blood[34,35]. Fate-mapping experiments show that nT_{reg} cells are quite stable under steady-

state conditions[20], whereas iT_{reg} cells are known to be unstable[14,15,19]. Under conditions of chronic inflammation, such as those that exist in atherosclerosis, exT_{reg} cells, that is, cells that no longer express FoxP3, are found routinely[4,14,16,17]. Zhou et al. showed the development and pathogenicity of exT_{reg} cells from T_{reg} cells using $Foxp3^{GFP}$ × $Rosa26^{-loxP\text{-}Stop\text{-}loxP\text{-}YFP}$ fate-mapping mice crossed with NOD mice[14]. We previously showed that exT_{reg} cells from mice, vaccinated with an apolipoprotein B peptide, produced IFN-γ[7]. Adoptive transfer of such exT_{reg} cells increased atherosclerotic lesion size[7].

Because the transcriptome of T_{reg} cells shares similarity with that of T_H17 cells[36,37], exT_{reg} cells were suspected to become T_H17 cells. We have previously shown that in women with cardiovascular disease, many APOB-specific T cells express both FoxP3 and RORγt[3]. This phenotype is consistent with T_{reg} cell plasticity, which proposes that T_{reg} cells acquire the transcriptional program of the cells they regulate[38,39]. Thus, T_H1-T_{reg} cells express T-bet, T_H17-T_{reg} cells express Stat3 and T_H2-T_{reg} cells express IRF4 (refs. 40–42). However, in atherosclerosis, T_{reg} cells lose FoxP3 expression. Based on flow cytometry, T_{reg} cells in atherosclerosis have been reported to become T_H17-like cells[3], T_H1-like cells[10,11] or T_{FH}-like cells[17]. Our present lineage tracking, gene and protein expression and functional data show that, in both mice and humans, exT_{reg} cells are cytotoxic $CD4^+$ T cells. The relationship between these different flavors of exT_{reg} cells remains to be explored.

Recent work has shown a loss of tolerance to self in mice[43] and humans[44] with atherosclerosis. Many T_{reg} cells express TCRs specific for self-epitopes[45]. Thus, it is plausible that the conversion of T_{reg} cells to exT_{reg} cells through proliferation and clonal expansion may be part of the mechanism for this loss of tolerance to self. The function of exT_{reg} cells includes cytotoxicity. In fact, CTLs have been reported in plaques[46]. exT_{reg} cells are also pro-inflammatory by attracting monocytes. Thus, exT_{reg} cells are expected to exacerbate atherosclerosis by attracting more monocytes, some of which can differentiate to macrophages[9].

Transcriptomic analysis, ICS and functional assays all show that exT_{reg} cells have a highly activated cytotoxic phenotype. However, exT_{reg} cells retain expression of the T_{reg} cell markers PD-1, GITR and TIGIT, and expression of some T_{reg} cell genes. TCRβ sequencing shows that exT_{reg} cells have a limited repertoire diversity and show clear clonal expansion of TCR sequence patterns also found in T_{reg} cells. Experimentally, we show that T_{reg} cells proliferate in mice with atherosclerosis. Considering these findings together, we hypothesize that the development of exT_{reg} cells in chronic inflammation may be driven by repetitive TCR stimulation. Repetitive TCR stimulation is known to lead to a T_{emra}-like phenotype[47]. Through this process, exT_{reg} cells become cytotoxic and pro-inflammatory T_{eff} cells.

It was surprising to find CD16 and CD56 as cognate surface markers for human exT_{reg} cells. CD56, also known as NCAM (neural cell adhesion molecule) and CD16, an Fc receptor (FcγRIIIa), are typically coexpressed on NK cells[48]. To contrast human exT_{reg} cells and NK cells, we compared their transcriptomes and found genes that were significantly differentially expressed in both mice and humans. We used FACS analysis to confirm the expression of T cell markers on $CD3^+CD4^+CD16^+CD56^+$ human exT_{reg} cells, which were

not detectable on $CD3^{-}CD4^{-}CD16^{+}CD56^{+}$ NK cells. Functionally, exT_{reg} cells, unlike NK cells, degranulated upon TCR engagement.

T_{reg} cells represent a unique, preexisting, non-naïve population of $CD4^{+}$T cells that have already been exposed to antigen. Unlike naïve T cells, T_{reg} cells can quickly respond to antigen exposure. In cancer models, T_{reg} cells play a role in shielding the tumor from the immune system. However, inhibiting indoleamine 2,3-dioxygenase drives some of these T_{reg} cells to provide CD40L-dependent help to dendritic cells for cross-presentation, thus licensing $CD8^{+}$T cells to become CTLs[49,50]. The reprogrammed T_{reg} cells were induced by vaccinating with antigen and a TLR9 ligand[50]. They arise from an Eos (Ikzf4)-labile population of T_{reg} cells[49]. Unlike the cytotoxic exT_{reg} cells identified here, the T_{reg} cells reprogrammed by indoleamine 2,3-dioxygenase inhibition still express FoxP3 at levels similar to T_{reg} cells[49]. Thus, these cells may represent early exT_{reg} cells, driven by adjuvant-induced inflammatory signals including IL-6 (ref. 50). In experiments using CFSE-labeled T_{reg} cells, reprogramming occurred at a time when proliferation was still minimal (that is, before proliferation) and required the IL-6 receptor on the T_{reg} cells[49]. The relationship between these early exT_{reg} cells and the cytotoxic exT_{reg} cells described here remains to be determined.

A limitation of this study is that the mouse exT_{reg} cell signatures are from sorted spleen and LN cells, while the human exT_{reg} cell transcriptomic data are from peripheral blood. This discrepancy is due to practical constraints. The yield of PBMCs in mice is insufficient for sorting T_{reg} cells and exT_{reg} cells for preparation of high-quality libraries. Conversely, LN or spleen biopsy samples are not available from the CAVA cohort (from where the human scRNA-seq dataset came). Future, more detailed studies, beyond the scope of this work, may yield more transcriptomic data for phenotypic and functional analysis.

In conclusion, we discovered and defined, phenotypically and functionally, human exT_{reg} cells. Although human exT_{reg} cells retain some T_{reg} cell markers, their main gene signature is cytotoxic. Functionally, human exT_{reg} cells kill target cells as efficiently as CTLs. exT_{reg} cells are pro-inflammatory in that they express IFN-γ and monocyte-attracting chemokines. The conversion of T_{reg} cells to exT_{reg} cells may be part of the recently described breaking of tolerance to self in atherosclerosis.

Online content

Any methods, additional references, Nature Portfolio reporting summaries, source data, extended data, supplementary information, acknowledgements, peer review information; details of author contributions and competing interests; and statements of data and code availability are available at https://doi.org/10.1038/s41590-023-01589-9.

Methods

Human samples

Healthy volunteers were recruited by the clinical core at the La Jolla Institute for Immunology (LJI). All participants received financial compensation according to guidelines approved by LJI's Institutional Review Board. Written informed consents were obtained

from all enrolled participants. Donors self-reported ethnicity and race details, and tested negative for hepatitis B, hepatitis C and HIV. None of the donors had any ongoing infection. They had no known conditions of cancer, diabetes, heart or kidney or liver disease. Donors were neither pregnant nor nursing. De-identified blood or PBMC samples for the study were made available by LJI's clinical core. Ethical approval for the study was provided by the Institutional Review Board of LJI (IRB protocol nos. IB-248–0821 and VD-057).

Animal experiments

All animal experiments in this study used fate-mapping lineage-tracker mice (*FoxP3*$^{eGFP\text{-}Cre\text{-}ERT2}$*ROSA26*$^{CAG\text{-}fl\text{-}stop\text{-}fl\text{-}tdTomato}$ *Apoe*$^{-/-}$ in a B6 background) from both sexes, as previously described[7]. All mouse experiments were approved by the LJI Animal Care and Use Committee (protocol no. AP00001019). The housing conditions for these mice were as follows: lights on at 6:00 and off at 18:00, ambient temperature between 20 °C and 24 °C and humidity between 30% and 70% (mean, 40%; outdoor environment can affect humidity inside).

Seven- to eight-week-old lineage-tracker mice were injected with tamoxifen for 5 consecutive days (intraperitoneally; 75 mg per kg body weight). For time-course experiments, spleens and LNs from four to seven mice (exact number indicated in figure legends) were harvested at 4, 8, 12 or 20 weeks after tamoxifen injection. Fixed samples of mouse carotid arteries from four 20-week-old tamoxifen-injected mice were imaged using a Leica SP8 confocal microscope with a HC Fluotar ×25/0.95 water objective. CD25 expression was quantified in single-cell suspensions from spleens ($n = 4$) and LNs ($n = 6$) of 16-week-old tamoxifen-injected mice. Bulk RNA-seq was performed on spleens ($n = 5$) and LNs ($n = 4$) from 20-week-old tamoxifen-injected mice. Animals were on a regular CD. For analysis of Foxp3/GFP and tdTomato/RFP within non-T cells, TCRβ^{+}CD4^{-} cells and TCRβ^{+}CD4^{+} cells, three 8-week-old female lineage-tracker mice were injected with tamoxifen twice for 5 d each, at week 1 and week 6. These mice were fed a western diet (WD; 42% kcal from fat, 0.2% cholesterol) for 12 weeks and then spleens ($n = 3$) and LNs ($n = 3$) were harvested for flow cytometry.

BrDU proliferation assay

Seven 8-week-old female *Foxp3*$^{eGFP\text{-}Cre\text{-}ERT2}$*ROSA26*$^{fl\text{-}STOP\text{-}fl\text{-}tdTomato}$ *Apoe*$^{-/-}$ (B6) mice were injected with tamoxifen twice for 5 d each, at week 1 and week 6, then fed a WD for 12 weeks. For six mice, BrDU (0.8 mg ml^{-1}) was incorporated in the drinking water for the last 9 d of WD feeding. Spleen cells were harvested and processed into single-cell suspensions. After staining for viability and surface markers for 30 min at 4 °C, cells were fixed and permeabilized for 20 min at 24 °C with the Foxp3-staining kit (eBioscience). Cells were then treated with DNase I solution for 1 h at 37 °C. Cells were washed and stained for intracellular markers for 30 min at 24 °C. Samples were analyzed on an LSR II (BD Biosciences).

Cell isolation

Mouse spleens and LNs were harvested, crushed and filtered through a sterile 100-μm filter in 1× PBS. Red blood cells and platelets from spleen cells were discarded using RBC lysis buffer (Invitrogen) for 5 min followed by centrifugation at 250*g* for 10 min.

hPBMCs were isolated by density gradient centrifugation. Briefly, undiluted blood was transferred onto Ficoll-PaquePLUS (Cytiva) in SepMate tubes (StemCell) and centrifuged at 1,200*g* for 10 min. PBMC ring was harvested, washed with 1× PBS (Gibco) and centrifuged at 800*g* for 10 min. Red blood cells and platelets were discarded using RBC lysis buffer (Invitrogen) for 5 min followed by centrifugation at 250*g* for 10 min.

Flow cytometry

Mouse splenocytes or lymphocytes and hPBMCs were incubated with fixable viability dye (Ghost Dye Violet 510; Tonbo Biosciences or zombie yellow; BioLegend) for 30 min at 4 °C, washed and antibodies against surface markers were added for 30 min at 4 °C, according to the analysis mentioned in the figure legends. ICS was performed using either the eBioscience IC Fixation Buffer (only cytokines or chemokine panels) or the eBioscience Foxp3/Transcription factor staining buffer set (when cytokines were co-stained with FOXP3) for 20 min at 24 °C. Briefly, cells were permeabilized, then incubated with antibodies against intracellular markers (as mentioned in the figure legends) for 45 min at 24 °C and analyzed on an LSR Fortessa or LSR II (BD Biosciences).

For suppressive assay readout, cells were incubated with anti-CD3 or anti-CD4 for 20 min at 4 °C. DAPI was added right before analyzing on a BD FACSCanto (BD Biosciences).

For ICS assay, hPBMCs were stimulated for 6 h with PMA and ionomycin (1×; Cell Stimulation Cocktail, eBioscience). For the last 4 h, protein transport inhibitors brefeldin and monensin (1×; Protein Transport Inhibitor Cocktail, eBioscience) were added. After staining for viability and surface markers, cells were fixed, permeabilized and stained for intracellular markers. Samples were analyzed on an LSR II (BD Biosciences). All flow cytometry data were analyzed using FlowJo version 10.8.1.

Antibodies used are listed in Supplementary Table 12.

Cell sorting

Mouse cells from spleens and LNs were first incubated with a fixable viability dye for 30 min at 4 °C, washed and antibodies against surface markers were added for 30 min at 4 °C. Cells were sorted with a FACSAria II (BD Biosciences). Mouse T_{reg} cells were defined as $TCR\beta^+CD4^+GFP^+TdTomato^+$ and exT_{reg} cells as $TCR\beta^+CD4^+$ $GFP^-TdTomato^+$. hPBMCs were first enriched for $CD4^+$ T cells. Cells were incubated with purified anti-CD14, anti-CD19 and anti-CD8a for 20 min at 4 °C. Then, Dynabeads coated with goat anti-Mouse IgG (Invitrogen) were added to the cells for 10 min on a turning wheel at 4 °C. Using a magnet, the supernatant containing CD4-enriched T cells was collected. Enriched cells were incubated for 30 min at 4 °C with antibodies against surface markers. Dead cells were stained using DAPI right before sorting on a FACSAria II or FACSAria Fusion (BD Biosciences). After gating on morphology, singlets, live cells ($DAPI^-$) and

CD8a^{-}CD14^{-}CD19^{-} T_{reg} cells were defined as CD3^{+}CD4^{+}CD25^{hi}CD127^{lo}, exT_{reg} cells as CD3^{+}CD4^{+}CD56^{+}CD16^{+} and naive T cells as CD3^{+}CD4^{+} CD45RA^{+}CCR7^{+}.

Antibodies used are listed in Supplementary Table 12.

Quantitative real-time PCR

Human T_{reg} cells and exT_{reg} cells were directly sorted into 750 µl TRIzol LS (Thermo Fisher) and 20 µl of low-input lysis buffer (0.1% Triton X-100 (vol/vol), 1 U µl^{-1} RNase inhibitor, 2.5 mM dNTP), respectively. For TRIzol samples, RNA was extracted with miRNAeasy micro kit (Qiagen). Total RNA was quantified using a nanodrop spectrophotometer. TRIzol and low-input samples were reverse transcribed into cDNA using SuperScript II reverse transcriptase (Thermo Fisher). Real-time PCR reactions were performed according to the RT2 SYBR green gene expression assay protocol (Qiagen). RT^2 SYBR Green qPCR master mix and premade RT^2 qPCR Primer Assays (Qiagen) for human *CST7* (GeneGlobe ID PPH05560E-200), *NKG7* (GeneGlobe ID PPH07745A-200), *GZMA* (GeneGlobe ID PPH00314F-200), *PRF1* (GeneGlobe ID PPH07126A-200), *TBX21* (GeneGlobe ID PPH00396A-200), *CCL4* (GeneGlobe ID PPH00563B-200) and *ACTB* (GeneGlobe ID PPH00073G-200) were used. Details can be found at https://geneglobe.qiagen.com/us/product-groups/rt2-qpcr-primer-assays. Results were calculated by applying the $1/^{\Delta CT}$ method using *ACTB* as housekeeping gene.

Bulk RNA-seq

Mouse T_{reg} cells and exT_{reg} cells were sorted into TRIzol LS (Thermo Fisher). Human T_{reg} cells (200,000–500,000) were sorted into 750 µl of TRIzol LS (Thermo Fisher), while human exT_{reg} cells (1,000 cells) were directly sorted in 20 µl of low-input lysis buffer as described previously[51]. For TRIzol samples, RNA was extracted using the miRNeasy micro kit (Qiagen). RNA quality was measured by using a 2100 TapeStation (Agilent Technologies). Samples with high-quality RNA (RNA integrity number > 8.0) were used for the next steps. For both TRIzol LS and low-input samples, double-stranded-cDNA was prepared using the SuperScript II reverse transcriptase (Thermo Fisher) according to the manufacturer's instructions. cDNA was amplified using 15 cycles and eluted in 24 µl. Around 100 ng of resulting cDNA was processed using the Illumina DNA Prep Kit (20018704, Illumina) following the manufacturer's instructions. Samples were normalized based on DNA concentration, pooled and loaded onto an Illumina NovaSeq 6000, and sequenced with 50 base-pair paired-end reads (PR50). Post-mapping quality-control checks were used to exclude poor-quality samples. Sequencing quality control was performed with FastQC v0.11.9 and MultiQC version v1.12. RNA-seq reads were trimmed using Ilumina's DRAGEN FASTQ toolkit version 1.0.0. The STAR (v2.7.1 with default parameters)[52] aligner was used to map the transcriptomes of the human and mouse bulk RNA-seq data to GENCODE GRCh38.p13 and GENCODE GRCm39, respectively. Raw read gene counts were obtained using STAR aligner with the '--quantMode GeneCounts' option, which was used for the differential gene expression analysis. Quality of read counts was assessed before normalization, batch-effect correction and performing differential expression analysis using DESeq2 (v1.34)[53]. To eliminate lowly expressed genes, a cutoff (≤100 raw counts across samples) was enforced to remove genes with low read counts. Normalized counts data from

DESeq2 were used to make *z*-score heat maps and perform the differential gene expression analysis. Variance stabilizing transformed (VST) counts were used to make the PCA plot and the spearman correlation plot.

Donor information is listed in Supplementary Table 13. Mouse and human bulk RNA-seq data are available on the NCBI Gene Expression Omnibus (GEO) under accession no. GSE217010.

Support vector machine

We used the SVM classifier from Scikit-learn (v1.1)[54] machine learning library to classify data points. Packages such as Numpy (v1.23.2), Matplotlib (v3.5.2), Pandas (v 1.4.3) and Seaborn (v0.11.2) were used along with Scikit-learn to aid preprocessing. The mouse bulk RNA-seq data on sorted exT_{reg} cells and T_{reg} cells from spleen and LNs were used for SVM classification. For binary classification purposes, samples were labeled as either exT_{reg} cells or T_{reg} cells. Information on tissue type was disregarded. In total, 383 overlapping mouse–human orthologous genes were used in the single-cell datasets. The linear kernel was used to make predictions for which data were split into 90% train and 10% test. Fivefold cross-validation resulted in an accuracy of ~98%. The feature weights were extracted from the linear classifier to interpret the weights assigned to the genes. The weights defined the classifying power of each gene. The top 60 genes with positive weights (classifying exT_{reg} cells) and the top 60 genes with negative weights (classifying T_{reg} cells) were identified.

Single-cell RNA-seq analysis

A published[21] single-cell dataset with CITE-seq on hPBMCs was used. This dataset is from 61 men and women (aged 40–80 years) undergoing cardiac catheterization at the University of Virginia Health System. All participants provided written informed consent before enrollment, and the study was approved by the Human Institutional Review Board (no. 15328) at the University of Virginia. Peripheral blood for sequencing experiments was obtained from these participants before catheterization. We performed differential gene expression analysis using Seurat v4.0.6 (FindAllMarkers and FindMarkers function), which uses the Wilcoxon rank-sum test. We compared these cells against all the $CD4^+$ T cells and the T_{reg} cells (cluster 17 from ref. 21) to identify DEGs and surface markers. Human scRNA-seq data are available at the NCBI GEO (accession no. GSE190570).

Plots

GGplot2 v3.3.5 and ComplexHeatmaps v2.12.1 were used to make bar plots and heat maps. Feature plots and UMAP plots were generated using Seurat's FeaturePlot and DimPlot functions. Dot plots were generated using the package Ggpubr v0.4.0.

Enrichment analysis

For pathways analysis, gene lists have been inputted to the Enrichr online tool (https://maayanlab.cloud/Enrichr/). GSEA[55] (v4.2.3) was used to identify cell clusters enriched for T cell-specific gene sets. We interrogated the pseudobulk of the single-cell transcriptome by performing GSEA against the exT_{reg} cell and T_{reg} cell gene signatures to identify clusters enriched for these cell types. We used the gene signatures of T_{reg} cells and exT_{reg} cells from

mouse and human bulk RNA-seq data to validate and characterize cells expressing these genes in the single-cell dataset.

Bulk TCRβ sequencing

Human T_{reg} cells, exT_{reg} cells and naive T cells were sorted in HEPES buffer (1× PBS with 2% FBS and 0.025 M HEPES, pH7.3) and gDNA was extracted using QIAamp DNA Micro Kit (Qiagen). TCRβ data were sequenced with the immunoSEQ assay (Adaptive Biotech). Processing of raw Illumina sequence reads, filtering, demultiplexing, clustering and mapping of CDR3 sequences and annotation of VDJ genes using IMGT (ImMunoGeneTics) database sequences were performed by Adaptive Biotechnologies. Final sequence data were made available for download and analysis with their immunoSEQ Analyzer. Details of all productive TCR sequences are provided in Supplementary Table 14. TCR data were analyzed using GLIPH (v.2)[22,56]. Further downstream analysis was done in R using packages dplyr v1.0.9 and stats v4.1.1. GLIPH clusters were filtered for Fisher's score < 0.05. Clonally expanded and enriched motifs were identified by *P*-value statistics using the poisson. test function to compare summed contribution scores of samples from each cluster (summed template frequency of each cell type by cluster). The poisson. test function performs an exact test of a simple null hypothesis about the ratio between two rate parameters. The $\log_2$ fold change values and *P* values of the enriched motifs were plotted as a volcano plot to identify expanded TCRs.

Donor information is listed in Supplementary Table 13.

Suppressive assay

Sorted $CD16^+CD56^+$ T cells and T_{reg} cells were labeled with CellTrace Violet (Thermo Fisher) and tested for suppressive activity at a ratio of T_{reg} cells/$CD16^+CD56^+$:Teff of 1:1 by a co-culture with CFSE labeled (Thermo Fisher) T_{eff} cells (12,500 cells per well) stimulated with the T_{reg} cell suppression inspector (Miltenyi) at a ratio of cells:beads of 1:2 in a 50 µl final volume of complete RPMI medium (RPMI 1640 medium + L-Glutamine, 1× penicillin–streptomycin, 10 mM HEPES buffer pH 7.3, 1 mM sodium pyruvate and 1× MEM non-essential amino acid) containing 5% AB Serum (GeminiBio). After 5 d of co-culture, proliferation was analyzed by dilution of CFSE in T_{eff} cells ($L/D^-CD3^+CD4^+$).

Degranulation assay

hPBMCs were co-cultured with P815 target cells at a 10:1 (PBMC:target) ratio for 6 h at 37 °C, 5% CO_2. Target cells were either pre-loaded with 5 µg ml^{-1} human anti-CD3 (OKT3 clone) or left uncoated. Fluorochrome-conjugated anti-CD107a was added to each well (1:100 dilution, vol/vol) at the start of the incubation period. After 2 h, protein transport inhibitor cocktail was added at a 1× concentration. After the incubation, cells were harvested, washed and stained with fluorescently labeled antibodies for surface markers. CD107a antibody was not added again at this stage. $CD16^+CD56^+$ exT_{reg} cells were gated from singlets, viable, $CD14^-$, $CD19^-$ $CD3^+CD4^+$T cells, while $CD16^+CD56^+$ mature NK cells were identified from $CD3^-CD4^-$ non-T cells.

Cytotoxic assay

P815 cells were incubated for 30 min with anti-CD3 (OKT3 clone; 5 μg ml^{-1}). After a washing step, cells were resuspended in complete RPMI medium containing 5% AB Serum and 50 μM β-mercaptoethanol. Sorted $CD8^+$ CTLs, T_{reg} cells and $CD16^+CD56^+$ T cells were co-cultured with anti-CD3-loaded P815 at a ratio of 1:5 of P815:effector cells (7,500 P815 cells per well) in a final volume of 50 μl for 16 h at 37 °C and 5% CO_2. Cytotoxicity was measured in the supernatant using CyQUANT LDH Cytotoxicity Assay Kit following the provider's instructions (Invitrogen).

Statistics

Data analysis and statistical comparisons were done using GraphPad Prism version 9.3.1 and R version 4.0.1. We used a two-tailed Wald test with Benjamini–Hochberg *P*-value adjustment for comparing differential expression of genes in the human and mouse bulk RNA-seq transcriptomes. For analysis of gene and surface marker enrichment within $CD4^+$ T cell clusters in the human scRNA-seq data, we used a two-tailed Wilcoxon's rank-sum test with Benjamini–Hochberg correction for multiple comparisons. We used a two-sided Poisson test for the identification of enriched CDR3 motifs in the human TCR-seq dataset. Two-sample comparisons were done with a two-tailed Mann–Whitney *U* test or with a two-tailed unpaired student's *t*-test. We used one-way ANOVA with Dunnett's multiple-comparison test or a Kruskal–Wallis test with Dunn's multiple-comparison testing for analyses involving more than two samples. A two-way ANOVA with Dunnett's multiple-comparison test was performed when two independent variables were involved. We used a two-tailed Fisher's exact test with Benjamini–Hochberg adjusted *P* values for pathway enrichment analysis. All statistical tests, sample sizes and error bar descriptions of graphs are detailed in the legends of respective figures. Statistical tests for supplementary tables are provided in the column headers. Exact *P* values are reported in the figure legends and Supplementary Information.

Reporting summary

Further information on research design is available in the Nature Portfolio Reporting Summary linked to this article.

Extended Data

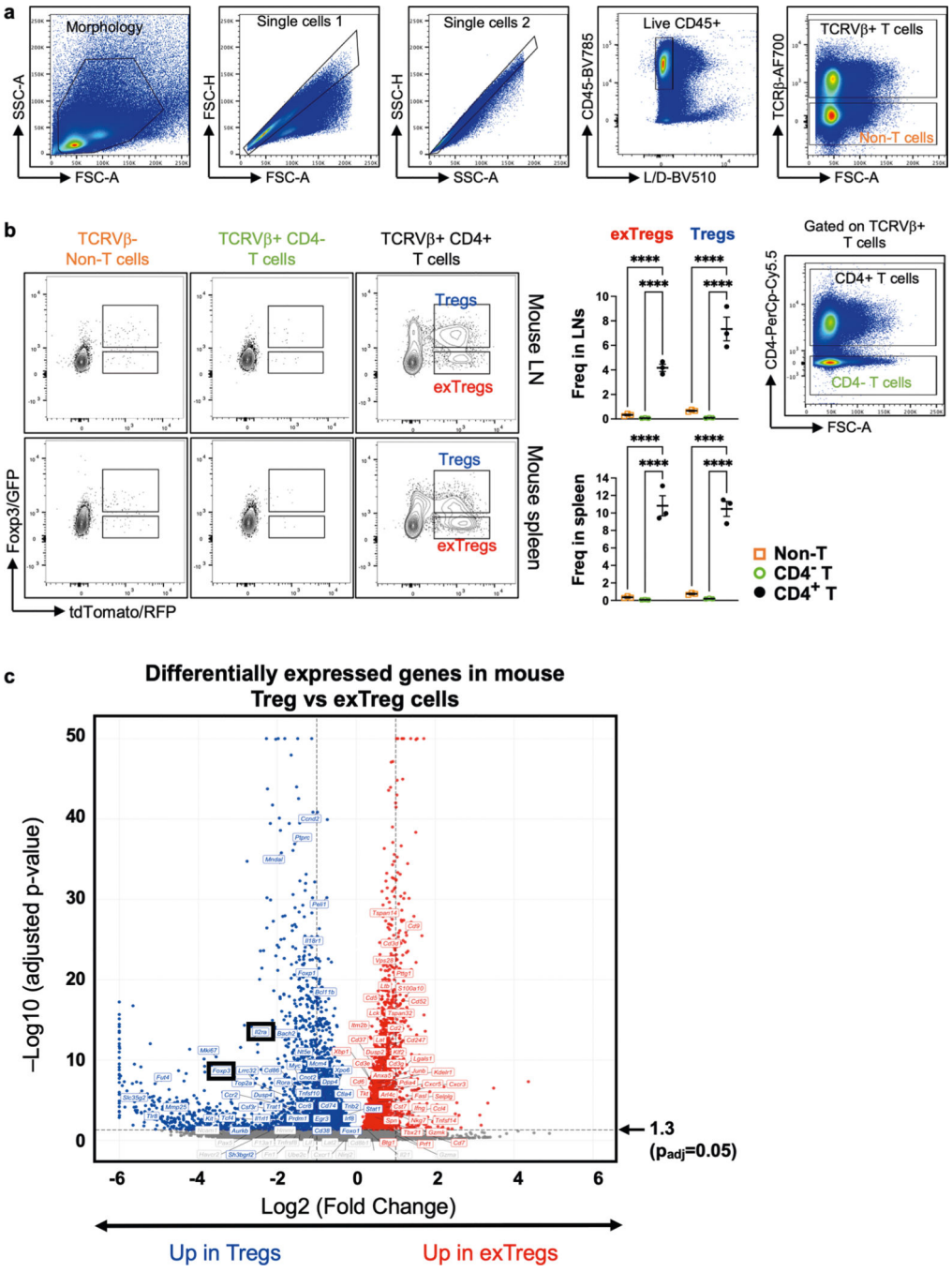

Extended Data Fig. 1 |. Experimental controls for lineage-tracker atherosclerotic mouse model and differentially expressed genes in mouse Treg cells vs exTregs.

(a,b) Eight week-old female *Foxp3*$^{eGFP\text{-}Cre\text{-}ERT2}$ *ROSA26*$^{fl\text{-}STOP\text{-}fl\text{-}tdTomato}$ *Apoe*$^{-/-}$ mice were injected with Tamoxifen twice for 5 days each, at week 1 and 6, then fed Western diet (WD) for 12 weeks. **a)** gating strategy, **b)** representative plots and quantification of exTreg and Treg cells among CD4^{+}T cells (black circles) in lymph nodes (LNs) and spleen, harvested after 12 weeks of WD from 3 independent mice. Non-T cells (orange

open squares) and CD4^{-}T cells (green open circles) are negative controls. Frequencies of exTregs and Treg cells among the parent subsets were plotted as mean ± SEM. Statistical comparisons were done using 2-way ANOVA with Dunnett's multiple comparison test. **** $p < 0.0001$. **c)** Volcano plot representing significantly differentially expressed genes between mouse Treg cells and exTregs from 20-week old *FoxP3*$^{eGFP\text{-}Cre\text{-}ERT2}$ *ROSA26*$^{CAG\text{-}fl\text{-}stop\text{-}fl\text{-}tdTomato}$ *Apoe*$^{-/-}$ mice (lymph nodes and spleen pooled). Left, up in Treg cells (blue). Right, up in exTregs (red). Horizontal dotted line is at $-\log_{10}$ (p adjusted) = 1.3 ($p_{adj} = 0.05$). The top 60 exTreg and 60 Treg classifying genes from the SVM model are annotated. Canonical Treg genes *Il2ra* and *Foxp3* are shown in black boxes. Statistical analyses of DE genes using two-tailed Wald test with Benjamini-Hochberg correction for multiple comparisons.

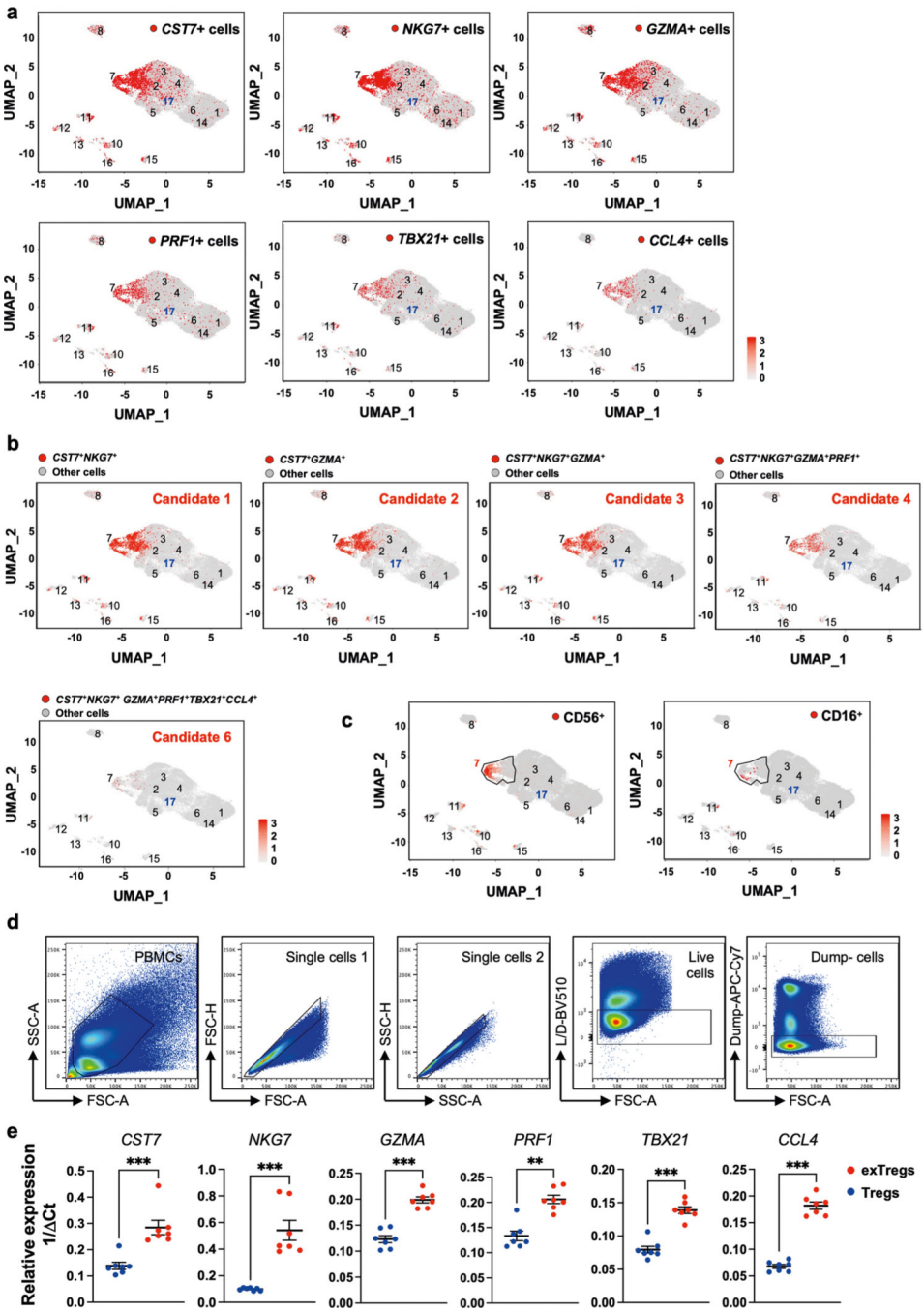

Extended Data Fig. 2 |. Expression of exTreg candidate genes in scRNAseq data and validation by qRT-PCR from sorted human cells.

(a) Feature maps showing the gene expression of the single gene markers *CST7, NKG7, GZMA, PRF1, TBX21* and *CCL4* in the human single-cell dataset for all CD4 T cell clusters. **(b)** Combinations 1–4 and 6 of exTreg candidate genes are highlighted in red on UMAP embeddings of CD4 T clusters from the scRNA-Seq. **(c)** UMAP embeddings of CD4 T clusters. Black outline marks cluster CD4T_7; cells that express either CD56 (left) or CD16 (right) are shown as red dots. **(d)** Gating strategy to identify exTreg and Treg cells

in human PBMCs. Dump channel: CD14, CD19. **(e)** Gene expression analysis of *CST7, NKG7, GZMA, PRF1, TBX21* and *CCL4* in sorted human Treg cells (blue circles) and exTregs (red circles) by qRT-PCR. Gene-specific Ct values were normalized (ΔCt) based on actin (*ACTB*). Relative expression was calculated by the 1/ΔCt method. n = 7. 33.33% male, 66.67% female donors; age: 21–54 yrs. Data shown as mean ± SEM. Each dot represents a biological replicate from an independent donor. Statistical comparisons by two-tailed Mann Whitney U test. **p = 0.0012,***p = 0.0006.

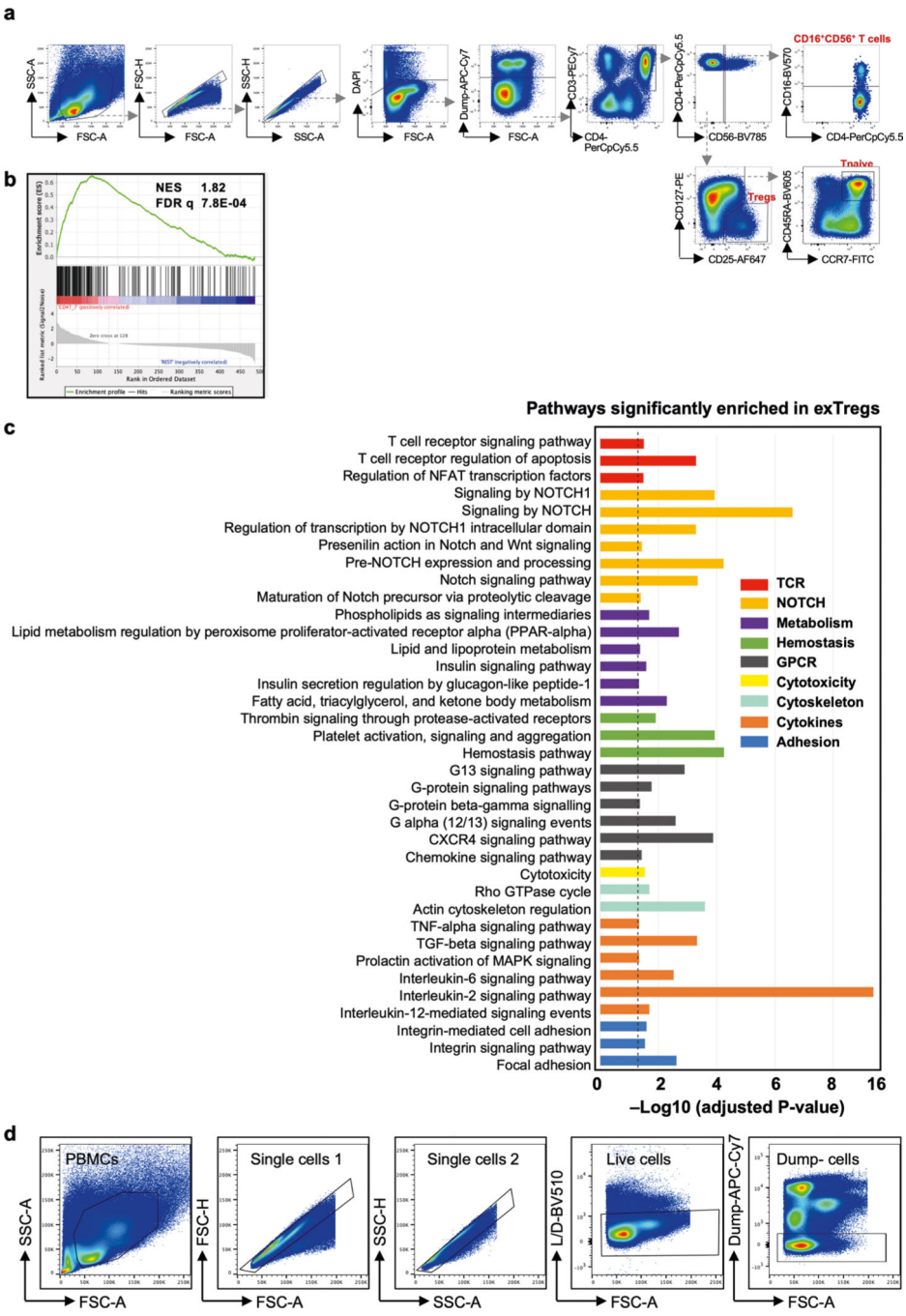

Extended Data Fig. 3 |. Human bulk RNAseq.

(a) Gating strategy used to sort human exTregs and Treg cells to perform bulk RNA-seq. **(b)** gene set enrichment analysis (GSEA) of bulk RNA-seq transcriptomes of sorted human exTreg cells against CD4T_7 (left) and all other clusters (right). Normalized enrichment score (NES) and FDR q values are indicated. **(c)** Significantly (adjusted $p < 0.05$) enriched pathways in human exTreg cells, based on genes expressed at significantly higher levels in human exTreg than in Treg cells. Analysis by Bioplanet2019 from the EnrichR suite. Dotted line indicates adjusted $p = 0.05$ ($-\log_{10}$ padj=1.3). Statistical comparisons with two-tailed Fisher's exact test and Benjamini- Hochberg adjustment of p-values. **(d)** Gating strategy to identify exTregs and NK cells in human PBMCs. Dump channel: CD14, CD19.

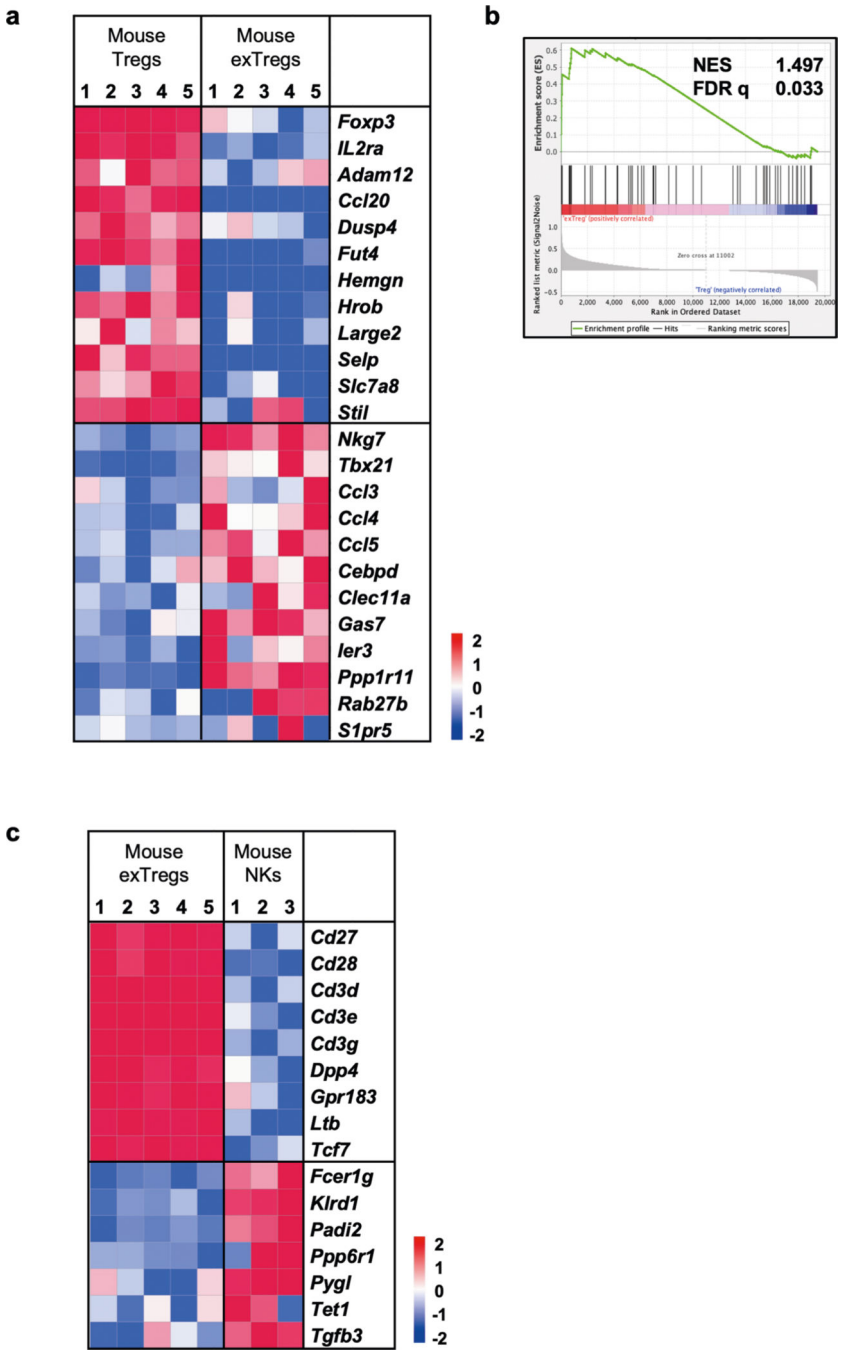

Extended Data Fig. 4 |. Mouse bulk RNAseq.

(a) Comparative gene signature analysis between mouse exTregs and Treg cells. Genes were filtered for significant differential expression in mouse and human dataset. Gene expression shown here is from *FoxP3*$^{eGFP\text{-}Cre\text{-}ERT2}$ *ROSA26*$^{CAG\text{-}fl\text{-}stop\text{-}fl\text{-}tdTomato}$ *Apoe*$^{-/-}$ mice. Low-expressed genes (<7 raw reads in all samples) in our dataset were filtered out. Technical replicates were averaged, biological replicates shown as columns. Analysis of differentially expressed (DE) genes was done using DESeq2. Curated list of significant DE ($log_2FC \pm 1$, adjusted $p < 0.05$) genes are shown on normalized heatmaps, scaled by row (z scores).

(b) Gene set enrichment analysis (GSEA) of mouse exTreg genes from bulk RNA-seq transcriptomes against human exTreg (left) and Treg cells (right) from the human bulk RNA-seq data set. Mouse orthologs of human genes, filtered for those present in the human scRNA-Seq targeted gene panel, were used to calculate enrichment for mouse bulk RNA-seq dataset. **(c)** Comparative gene signature analysis between mouse exTreg and NK cells. An external dataset was used for mouse NK cells (3 samples): GSE122597, GSE116177, and GSE52043. EdgeR was used to normalize the counts by applying the trimmed mean of M-values (TMM) method and counts per million (CPM) conversion. All other data processing and filtering steps were same as in a. Curated list of significant DE ($log_2FC \pm 1$, adjusted $p < 0.05$) genes are shown on normalized heatmaps, scaled by row (z scores). Statistical analyses of DE genes (a,c) using two-tailed Wald test with Benjamini-Hochberg correction for p-value adjustment. All data from independent biological replicates.

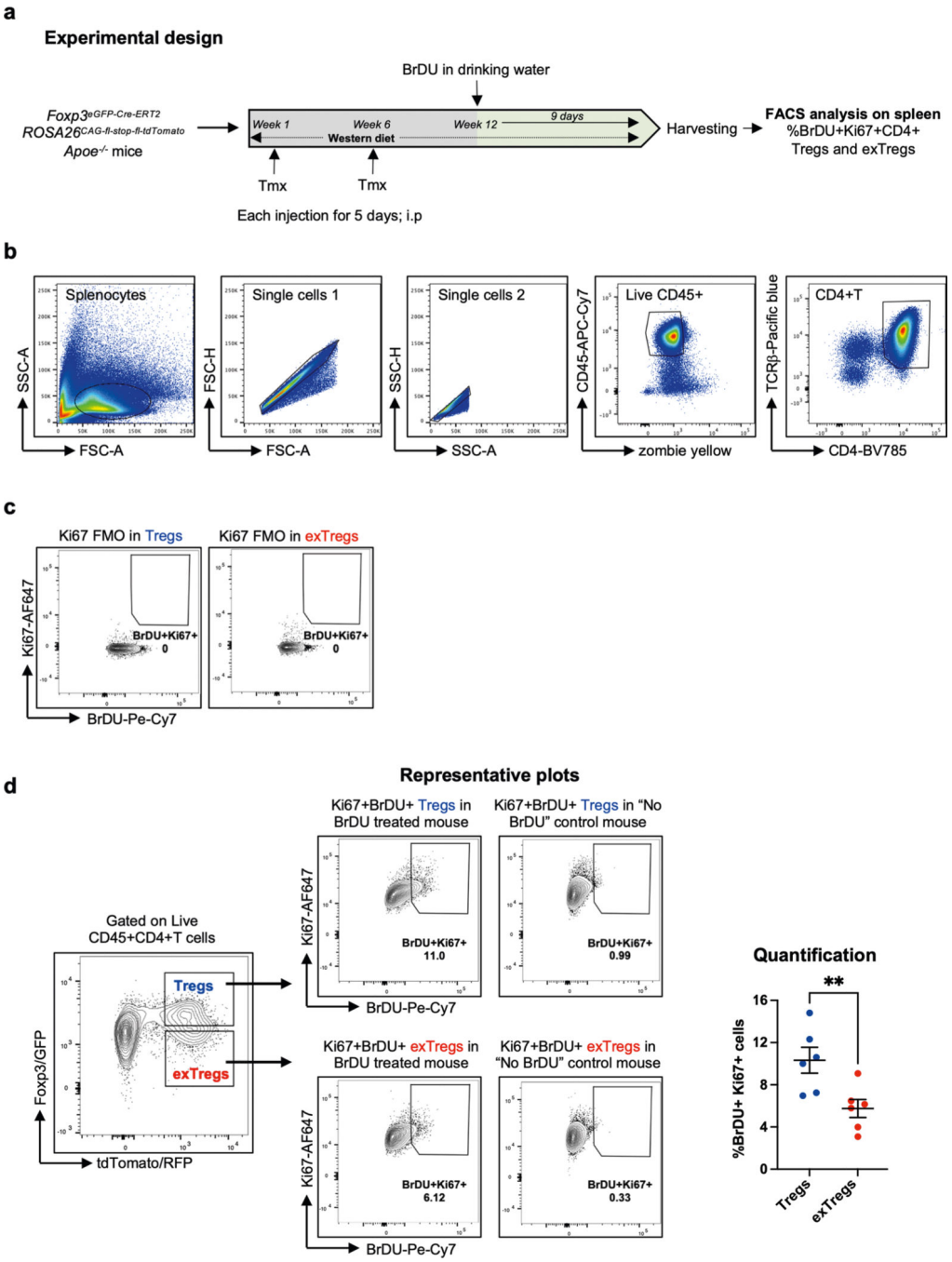

Extended Data Fig. 5 |. Assessment of proliferation in mouse Treg cells and exTregs.

(a) Eight week-old female *Foxp3*$^{eGFP\text{-}Cre\text{-}ERT2}$ *ROSA26*$^{fl\text{-}STOP\text{-}fl\text{-}tdTomato}$ *Apoe*$^{-/-}$ mice were injected with Tamoxifen twice for 5 days each, at week 1 and 6, then fed Western diet (WD) for 12 weeks. BrDU (0.8 mg/mL) was incorporated in the drinking water for the last 9 days of WD (n = 6). **(b)** Gating scheme for CD4^{+}T cells. **(c)** Ki67 FMO control. **(d)** Representative plots and quantification of proliferating Treg cells (blue circles, %Ki67^{+}BrDU^{+}CD4^{+}Foxp3^{+}RFP^{+}) and exTregs (red circles, %Ki67^{+}BrDU^{+}CD4^{+}Foxp3^{-}RFP^{+}) in the spleen (n = 6), as identified by anti-BrDU and

anti-Ki-67 Abs. Data shown as mean ± SEM. Each animal is an independent biological replicate. Gates were set by FMO for Ki67 and by no BrdU controls for BrdU. Background from “No BrDU” control was subtracted for normalization. The percentage of proliferating cells was compared by two-tailed Mann-Whitney U test, **p = 0.0087.

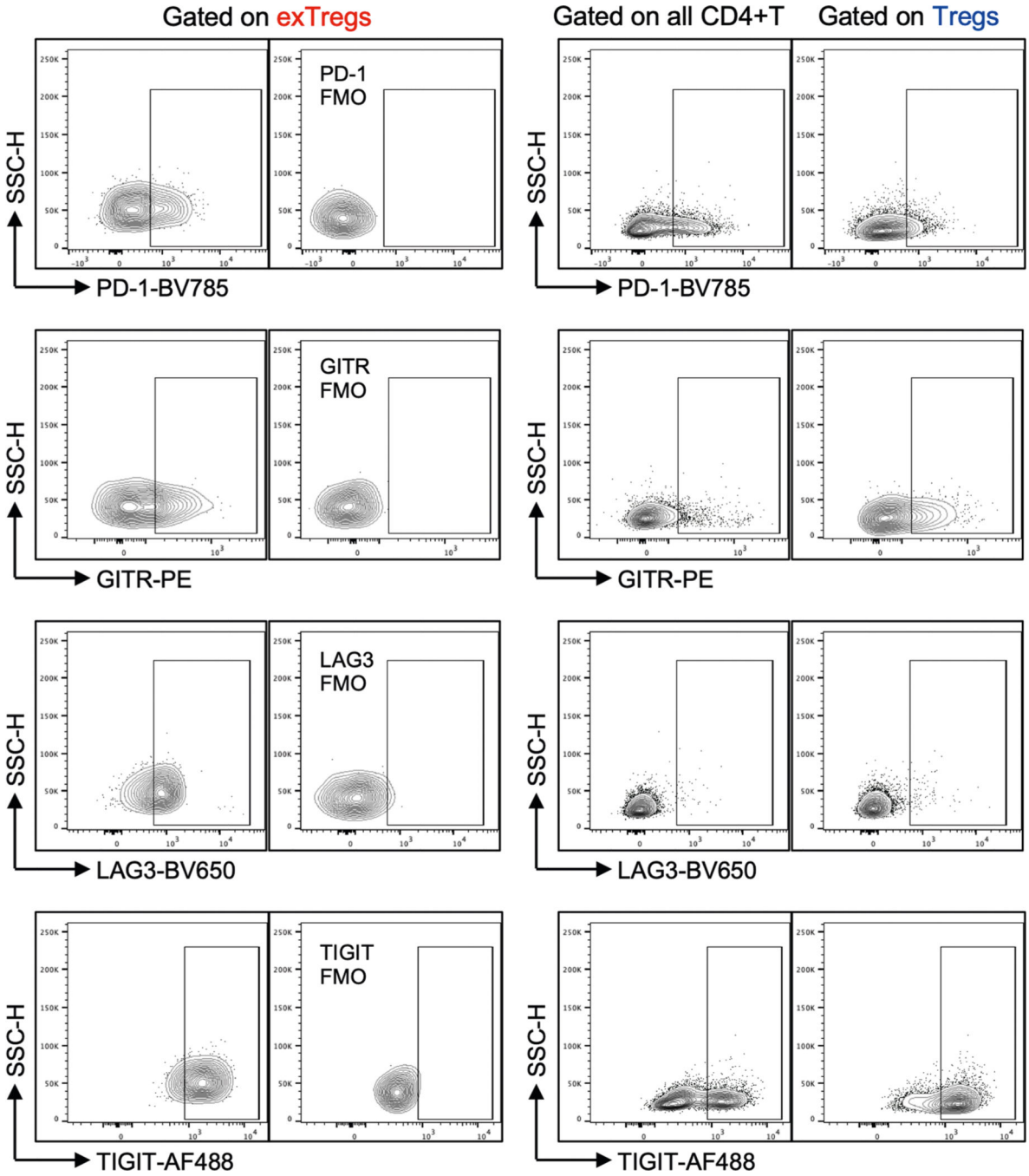

Extended Data Fig. 6 |. Treg marker expression on human exTregs.

Representative contour FACS plots showing the expressions of PD-1, GITR, LAG3 and TIGIT in exTreg cells (left). Corresponding FMO controls were used to set the gates. Right,

contour plots showing the expression of these markers in all $CD4^+$T cells and in Treg cells from the same donor.

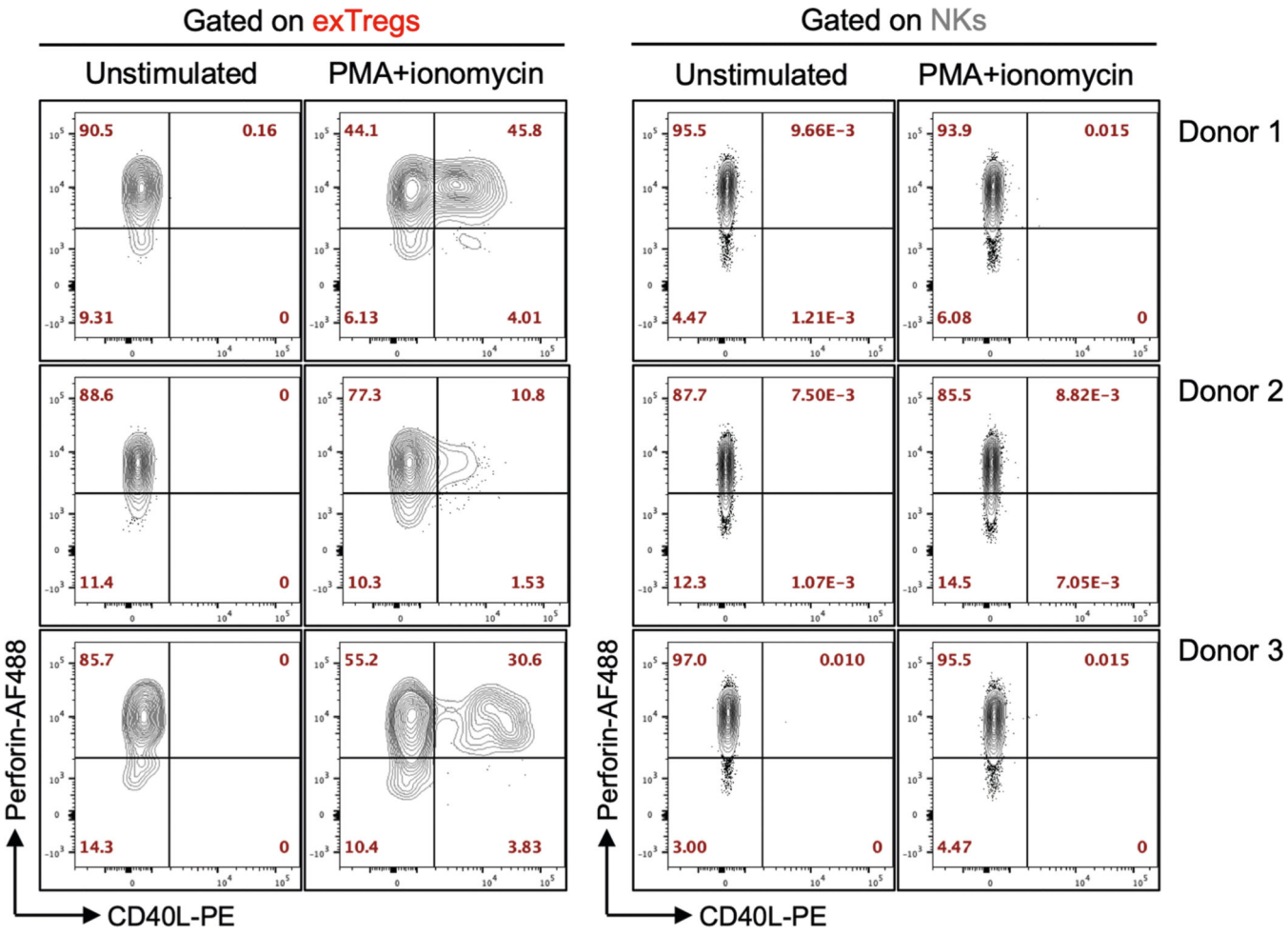

Extended Data Fig. 7 |. Cytotoxic and T cell activation marker expression on stimulated human exTreg vs NK cells.

Contour plots show intracellular expression of CD40L (X-axis) and Perforin (Y-axis) in exTregs and NK cells from unstimulated and PMA+ionomycin stimulated PBMCs. Data from three independent donors. 33.33% male, 66.67% female donors, age: 25–43 yrs.

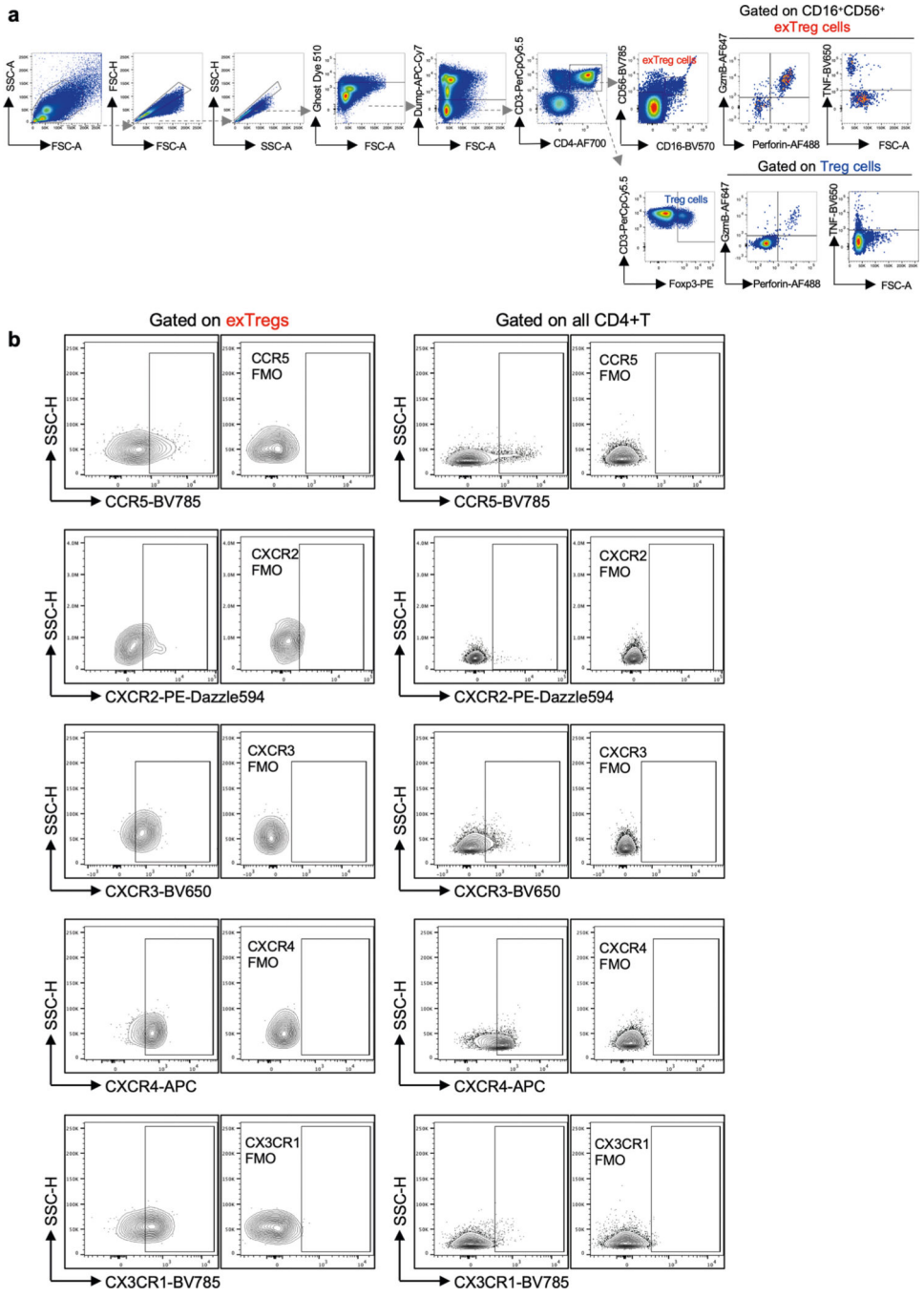

Extended Data Fig. 8 |. Gating strategy and representative plots.

(a) Gating strategy used to analyze granzyme B, perforin and TNF in Treg cells and exTregs. **(b)** Contour plots show surface expression of chemokine receptors CCR5, CXCR2, CXCR3, CXCR4 and CX3CR1 on exTreg cells (left) and their corresponding expression in all $CD4^{+}$T cells (right). Individual FMO controls were used to set the gate for expression of each receptor.

Supplementary Material

Refer to Web version on PubMed Central for supplementary material.

Acknowledgements

We thank A. Rudensky at Memorial Sloan Kettering Cancer Center for providing lineage-tracker mice. We also thank members of the clinical core and flow cytometry core at LJI. We thank Z. Mikulski and S. McArdle, microscopy core, LJI, for capturing images of exT_{reg} cells and T_{reg} cells in mouse arteries. We thank H. Cheroutre and N. Thiault who kindly provided the P815 cell line.

Data availability

RNA-seq data have been uploaded to the NCBI GEO and are accessible under accession numbers GSE217010 (mouse and human bulk RNA-seq) and GSE190570 (human scRNA-seq data). Human TCR-seq data were generated and processed by Adaptive Biotechnologies. Details of productive TCR sequences, accessed through their immunoSEQ Analyzer portal, are provided in Supplementary Table 14. Source data are provided with this paper.

References

1. Tse K. et al. Atheroprotective vaccination with MHC-II restricted peptides from ApoB-100. Front. Immunol 4, 493 (2013). [PubMed: 24416033]
2. Kimura T. et al. Atheroprotective vaccination with MHC-II-restricted ApoB peptides induces peritoneal IL-10-producing CD4 T cells. Am. J. Physiol 312, H781–H790 (2017).
3. Kimura T. et al. Regulatory $CD4^+$ T cells recognize major histocompatibility complex class II molecule-restricted peptide epitopes of apolipoprotein B. Circulation 138, 1130–1143 (2018). [PubMed: 29588316]
4. Wolf D. et al. Pathogenic autoimmunity in atherosclerosis evolves from initially protective apolipoprotein B 100 –reactive CD4+ T-regulatory cells. Circulation 142, 1279–1293 (2020). [PubMed: 32703007]
5. Marchini T, Hansen S. & Wolf D. ApoB-specific $CD4^+$ T cells in mouse and human atherosclerosis. Cells 10, 446 (2021). [PubMed: 33669769]
6. Roy P. et al. Immunodominant MHC-II (major histocompatibility complex II) restricted epitopes in human apolipoprotein B. Circ. Res 131, 258–276 (2022). [PubMed: 35766025]
7. Saigusa R. et al. Single-cell transcriptomics and TCR reconstruction reveal CD4 T cell response to MHC-II-restricted APOB epitope in human cardiovascular disease. Nat. Cardiovasc. Res 1, 462–475 (2022). [PubMed: 35990517]
8. Ait-Oufella H, Lavillegrand J-R & Tedgui A. Regulatory T cell-enhancing therapies to treat atherosclerosis. Cells 10, 723 (2021). [PubMed: 33805071]
9. Roy P, Orecchioni M. & Ley K. How the immune system shapes atherosclerosis: roles of innate and adaptive immunity. Nat. Rev. Immunol 22, 251–265 (2022). [PubMed: 34389841]
10. Li J. et al. $CCR5^+$T-$bet^+$$FoxP3^+$ effector CD4 T cells drive atherosclerosis. Circ. Res 118, 1540–1552 (2016). [PubMed: 27021296]
11. Butcher MJ et al. Atherosclerosis-driven T_{reg} plasticity results in formation of a dysfunctional subset of plastic IFNγ^+ T_h1/T_{regs}. Circ. Res 119, 1190–1203 (2016). [PubMed: 27635087]
12. Qiu R. et al. Regulatory T cell plasticity and stability and autoimmune diseases. Clin. Rev. Allergy Immunol. 58, 52–70 (2020). [PubMed: 30449014]
13. Ali AJ, Makings J. & Ley K. Regulatory T cell stability and plasticity in atherosclerosis. Cells 9, 2665 (2020). [PubMed: 33322482]
14. Zhou X. et al. Instability of the transcription factor Foxp3 leads to the generation of pathogenic memory T cells in vivo. Nat. Immunol 10, 1000–1007 (2009). [PubMed: 19633673]

15. Bailey-Bucktrout SL et al. Self-antigen-driven activation induces instability of regulatory T cells during an inflammatory autoimmune response. Immunity 39, 949–962 (2013). [PubMed: 24238343]
16. Svensson MND et al. Reduced expression of phosphatase PTPN2 promotes pathogenic conversion of T_{regs} in autoimmunity. J. Clin. Invest 129, 1193–1210 (2019). [PubMed: 30620725]
17. Gaddis DE et al. Apolipoprotein AI prevents regulatory to follicular helper T cell switching during atherosclerosis. Nat. Commun 9, 1095 (2018). [PubMed: 29545616]
18. Hsieh W-C et al. PTPN2 links colonic and joint inflammation in experimental autoimmune arthritis. JCI Insight 5, e141868 (2020).
19. Hua J. et al. Pathological conversion of regulatory T cells is associated with loss of allotolerance. Sci. Rep 8, 7059 (2018). [PubMed: 29728574]
20. Rubtsov YP et al. Stability of the regulatory T cell lineage in vivo. Science 329, 1667–1671 (2010). [PubMed: 20929851]
21. Saigusa R. et al. Sex differences in coronary artery disease and diabetes revealed by scRNA-seq and CITE-seq of human $CD4^+$ T cells. Int. J. Mol. Sci 23, 9875 (2022). [PubMed: 36077273]
22. Glanville J. et al. Identifying specificity groups in the T cell receptor repertoire. Nature 547, 94–98 (2017). [PubMed: 28636589]
23. Dogra P. et al. Tissue determinants of human NK cell development, function, and residence. Cell 180, 749–763 (2020). [PubMed: 32059780]
24. Ferraro A. et al. Interindividual variation in human T regulatory cells. Proc. Natl Acad. Sci. USA 111, E1111–E1120 (2014). [PubMed: 24610777]
25. Sokol CL & Luster AD The chemokine system in innate immunity. Cold Spring Harb. Perspect. Biol 7, a016303 (2015).
26. Mackay CR $CXCR3^+CCR5^+$ T cells and autoimmune diseases: guilty as charged? J. Clin. Invest 124, 3682–3684 (2014). [PubMed: 25180533]
27. Khaw YM et al. Astrocytes lure CXCR2-expressing $CD4^+$ T cells to gray matter via TAK1-mediated chemokine production in a mouse model of multiple sclerosis. Proc. Natl Acad. Sci. USA 118, e2017213118 (2021).
28. Weiskopf D. et al. Dengue virus infection elicits highly polarized $CX3CR1^+$ cytotoxic $CD4^+$ T cells associated with protective immunity. Proc. Natl Acad. Sci. USA 112, E4256–E4263 (2015). [PubMed: 26195744]
29. Stolla M. et al. Fractalkine is expressed in early and advanced atherosclerotic lesions and supports monocyte recruitment via CX3CR1. PLoS ONE 7, e43572 (2012).
30. Lesnik P, Haskell CA & Charo IF Decreased atherosclerosis in $CX3CR1^{-/-}$ mice reveals a role for fractalkine in atherogenesis. J. Clin. Invest 111, 333–340 (2003). [PubMed: 12569158]
31. Abi-Younes S. et al. The stromal cell-derived factor-1 chemokine is a potent platelet agonist highly expressed in atherosclerotic plaques. Circ. Res 86, 131–138 (2000). [PubMed: 10666407]
32. Shevach EM $Foxp3^+$ T regulatory cells: still many unanswered questions–a perspective after 20 years of study. Front. Immunol 9, 1048 (2018). [PubMed: 29868011]
33. Klein L, Robey EA & Hsieh C-S Central $CD4^+$ T cell tolerance: deletion versus regulatory T cell differentiation. Nat. Rev. Immunol 19, 7–18 (2019). [PubMed: 30420705]
34. Cording S. et al. The intestinal micro-environment imprints stromal cells to promote efficient Treg induction in gut-draining lymph nodes. Mucosal Immunol. 7, 359–368 (2014). [PubMed: 23945546]
35. Pezoldt J. et al. Neonatally imprinted stromal cell subsets induce tolerogenic dendritic cells in mesenteric lymph nodes. Nat. Commun 9, 3903 (2018). [PubMed: 30254319]
36. Bettelli E. et al. Reciprocal developmental pathways for the generation of pathogenic effector T_H17 and regulatory T cells. Nature 441, 235–238 (2006). [PubMed: 16648838]
37. Korn T. et al. IL-6 controls T_h17 immunity in vivo by inhibiting the conversion of conventional T cells into $Foxp3^+$ regulatory T cells. Proc. Natl Acad. Sci. USA 105, 18460–18465 (2008). [PubMed: 19015529]
38. Josefowicz SZ, Lu L-F & Rudensky AY Regulatory T cells: mechanisms of differentiation and function. Annu. Rev. Immunol 30, 531–564 (2012). [PubMed: 22224781]

39. Josefowicz SZ et al. Extrathymically generated regulatory T cells control mucosal T_H2 inflammation. Nature 482, 395–399 (2012). [PubMed: 22318520]
40. Chaudhry A. et al. $CD4^+$ regulatory T cells control T_H17 responses in a Stat3-dependent manner. Science 326, 986–991 (2009). [PubMed: 19797626]
41. Zheng Y. et al. Regulatory T-cell suppressor program co-opts transcription factor IRF4 to control T_H2 responses. Nature 458, 351–356 (2009). [PubMed: 19182775]
42. Koch MA et al. T-bet^+ T_{reg} cells undergo abortive T_h1 cell differentiation due to impaired expression of IL-12 receptor β2. Immunity 37, 501–510 (2012). [PubMed: 22960221]
43. Wang Z. et al. Pairing of single-cell RNA analysis and T cell antigen receptor profiling indicates breakdown of T cell tolerance checkpoints in atherosclerosis. Nat. Cardiovasc. Res 2, 290–306 (2023). [PubMed: 37621765]
44. Depuydt MAC et al. Single-cell T cell receptor sequencing of paired human atherosclerotic plaques and blood reveals autoimmune-like features of expanded effector T cells. Nat. Cardiovasc. Res 2, 112–125 (2023).
45. Fisson S. et al. Continuous activation of autoreactive $CD4^+$ $CD25^+$ regulatory T cells in the steady state. J. Exp. Med 198, 737–746 (2003). [PubMed: 12939344]
46. Chowdhury RR et al. Human coronary plaque T cells are clonal and cross-react to virus and self. Circ. Res 130, 1510–1530 (2022). [PubMed: 35430876]
47. Thome JJC & Farber DL Emerging concepts in tissue-resident T cells: lessons from humans. Trends Immunol. 36, 428–435 (2015). [PubMed: 26072286]
48. Van Acker HH, Capsomidis A, Smits EL & Van Tendeloo VF CD56 in the immune system: more than a marker for cytotoxicity? Front. Immunol 8, 892 (2017). [PubMed: 28791027]
49. Sharma MD et al. An inherently bifunctional subset of $Foxp3^+$ T helper cells is controlled by the transcription factor Eos. Immunity 38, 998–1012 (2013). [PubMed: 23684987]
50. Sharma MD et al. Reprogrammed $foxp3^+$ regulatory T cells provide essential help to support cross-presentation and $CD8^+$ T cell priming in naive mice. Immunity 33, 942–954 (2010). [PubMed: 21145762]
51. Rosales SL et al. A sensitive and integrated approach to profile messenger RNA from samples with low cell numbers. *Methods* Mol. Biol 1799, 275–302 (2018).
52. Dobin A. et al. STAR: ultrafast universal RNA-seq aligner. Bioinformatics 29, 15–21 (2013). [PubMed: 23104886]
53. Love MI, Huber W. & Anders S. Moderated estimation of fold change and dispersion for RNA-seq data with DESeq2. Genome Biol. 15, 550 (2014). [PubMed: 25516281]
54. Pedregosa F. et al. Scikit-learn: machine learning in Python. J. Mach. Learn. Res 12, 2825–2830 (2011).
55. Subramanian A. et al. Gene-set enrichment analysis: a knowledge-based approach for interpreting genome-wide expression profiles. Proc. Natl Acad. Sci. USA 102, 15545–15550 (2005). [PubMed: 16199517]
56. Huang H, Wang C, Rubelt F, Scriba TJ & Davis MM Analyzing the *Mycobacterium tuberculosis* immune response by T cell receptor clustering with GLIPH2 and genome-wide antigen screening. Nat. Biotechnol 38, 1194–1202 (2020). [PubMed: 32341563]

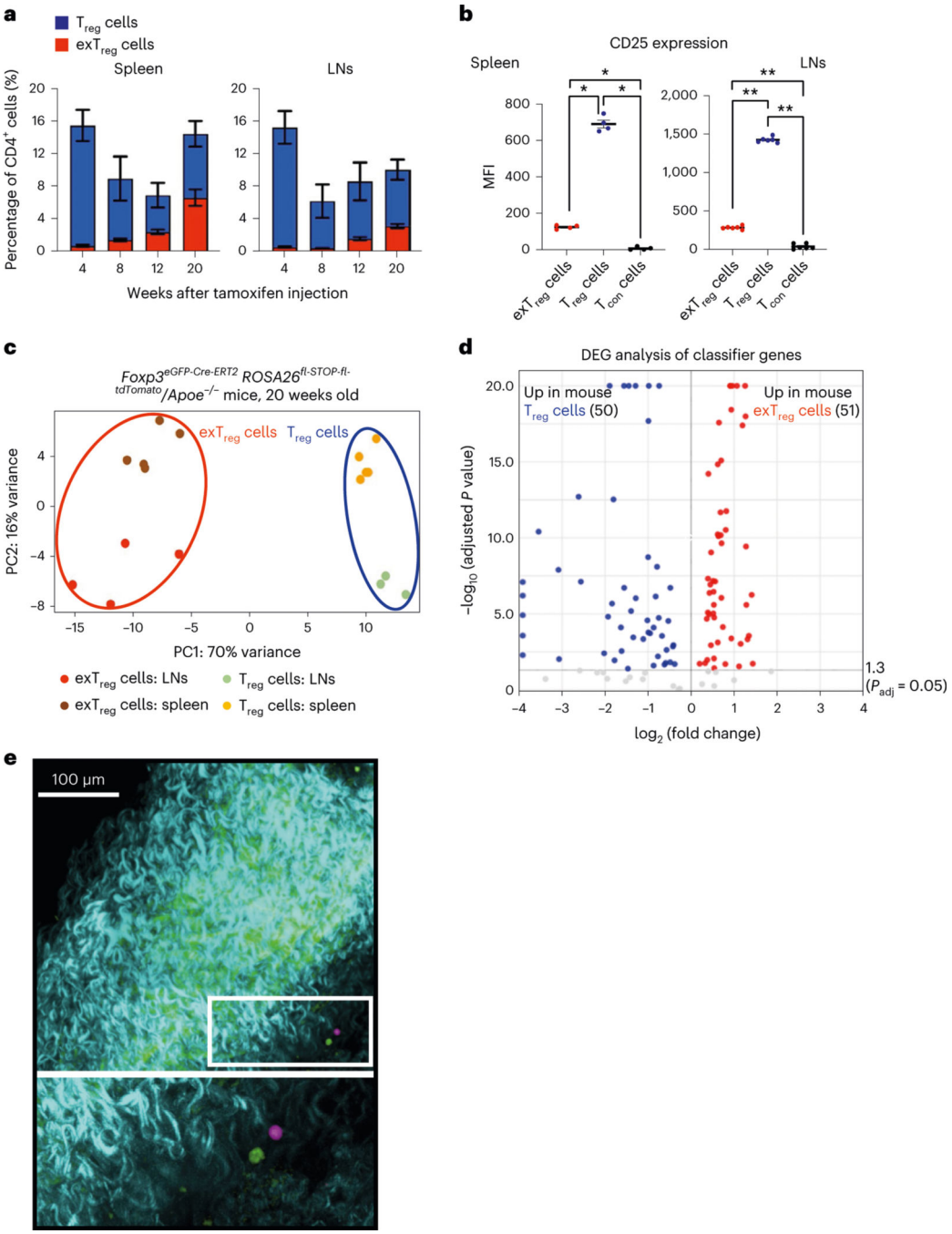

Fig. 1 |. Deep transcriptomes from mouse exT$_{reg}$ cells and T$_{reg}$ cells identify differentially expressed candidate genes.

a, Frequency of mouse exT$_{reg}$ cells (red) and T$_{reg}$ cells (blue) among all CD4$^+$T cells in spleen and LNs of *FoxP3$^{eGFP\text{-}Cre\text{-}ERT2}$ROSA26$^{CAG\text{-}fl\text{-}stop\text{-}fl\text{-}tdTomato}$ Apoe$^{-/-}$* mice at 4 (T$_{reg}$ $n = 7$; exT$_{reg}$ $n = 5$), 8 (T$_{reg}$ $n = 4$; exT$_{reg}$ $n = 4$), 12 (T$_{reg}$ $n = 5$; exT$_{reg}$ $n = 5$) and 20 (T$_{reg}$ $n = 6$; exT$_{reg}$ $n = 5$) weeks after tamoxifen injection. All mice were on regular CD. **b**, Median fluorescence intensity (MFI) of CD25 expression on exT$_{reg}$ cells (red circles), T$_{reg}$ cells (blue circles) and conventional CD4$^+$T cells (T$_{con}$, black circles) in spleen (*n*

= 4) and LNs (n = 6) from 16-week-old *FoxP3*$^{eGFP\text{-}Cre\text{-}ERT2}$*ROSA26*$^{CAG\text{-}fl\text{-}stop\text{-}fl\text{-}tdTomato}$ *Apoe*$^{-/-}$ mice on CD. Results (**a** and **b**) are represented as the mean ± s.e.m. Spleen (**b**) *P = 0.0286; LN (**b**) **P = 0.0022; two-tailed Mann–Whitney U test. **c**, PCA of bulk RNA-seq data from sorted mouse exT$_{reg}$ cells and T$_{reg}$ cells from spleen and LNs of 20-week-old *FoxP3*$^{eGFP\text{-}Cre\text{-}ERT2}$*ROSA26*$^{CAG\text{-}fl\text{-}stop\text{-}fl\text{-}tdTomato}$ *Apoe*$^{-/-}$ mice on CD. Results (**a**–**c**) are from independent biological replicates. **d**, Volcano plot of differentially expressed mouse exT$_{reg}$ and T$_{reg}$ cell-classifying genes, identified by the SVM trained on mouse transcripts with human orthologs and filtered for those present in the human scRNA-seq targeted gene panel. y and x axes capped at 20 ($P = 10^{-20}$) and ±4 ($\log_2$FC), respectively. Horizontal line at $-\log_{10}$ (P adjusted) = 1.3 (same as P_{adj} = 0.05). Statistical analyses were performed using a two-tailed Wald test with Benjamini–Hochberg P-value adjustment. **e**, Mouse aortas with carotid artery branches from *FoxP3*$^{eGFP\text{-}Cre\text{-}ERT2}$*ROSA26*$^{CAG\text{-}fl\text{-}stop\text{-}fl\text{-}tdTomato}$ *Apoe*$^{-/-}$ mice were fixed and imaged using a Leica SP8 multiphoton microscope. GFP$^+$ T$_{reg}$ cells (pseudocolored green) and tdTomato$^+$ exT$_{reg}$ cells (pseudocolored pink) in the adventitia (top). Bottom image is a zoomed-in view of the white box. Blue-green indicates a second harmonic generation microscopy analysis of extracellular matrix. Scale bar, 100 μm. Data are representative of four independent experiments.

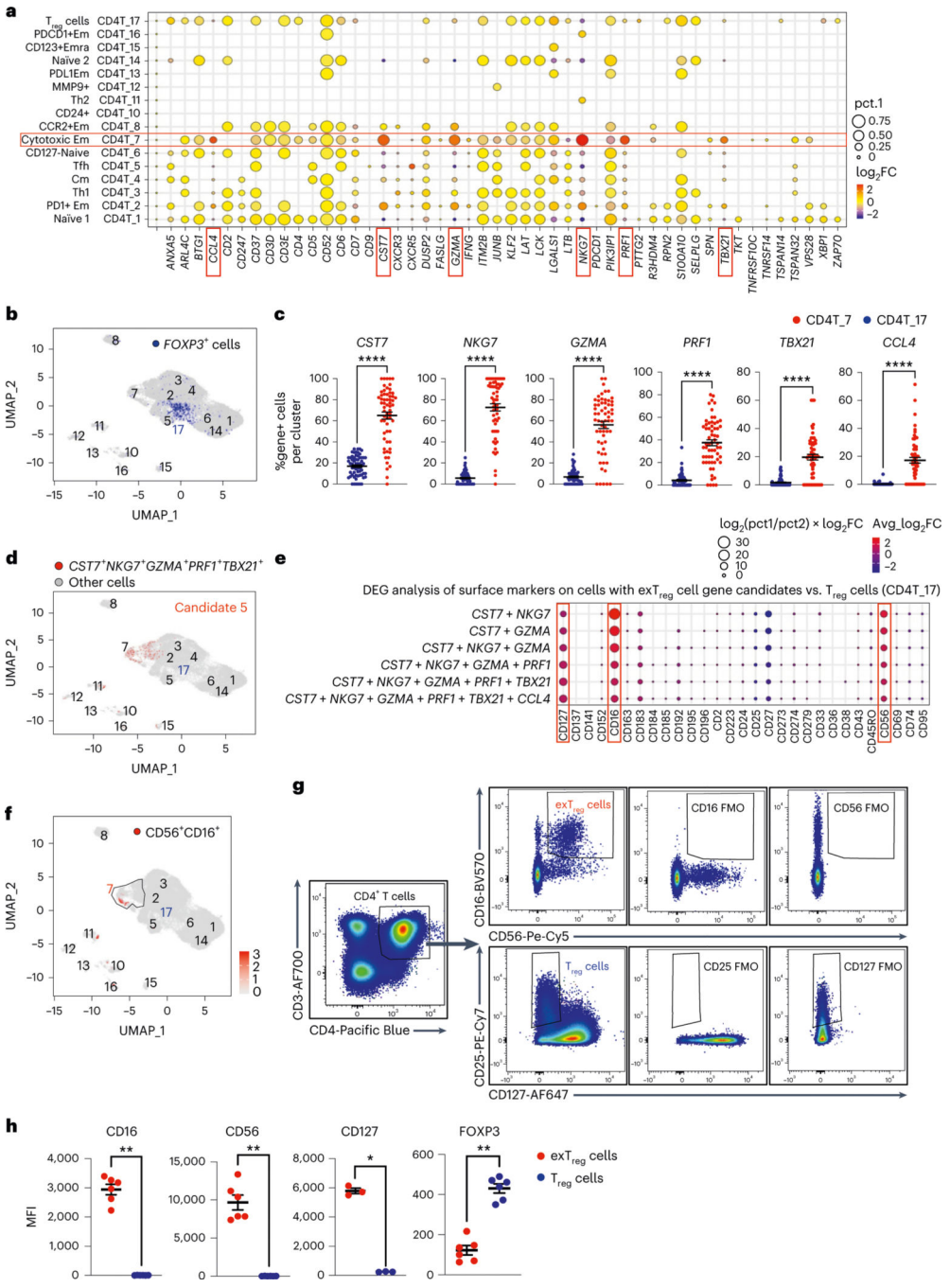

Fig. 2 |. Mouse exT$_{reg}$ cell classifier genes identify human exT$_{reg}$ cell candidate genes and surface markers in a human scRNA-seq and CITE-seq dataset of CD4$^+$T cells.

a, Differentially expressed mouse exT$_{reg}$ classifier genes were examined among all CD4$^+$ T cell clusters from a published single-cell human dataset from 61 men and women (aged 40–80 years). Statistical significance for the enrichment of each gene in one cluster versus all others was assessed. Average $\log_2$ fold change ($\log_2$FC, dot color) and positive cell proportions (pct.1, dot size) for significantly ($P < 0.05$) enriched genes are shown. Six highly expressed exT$_{reg}$ genes (*CST7*, *NKG7*, *GZMA*, *PRF1*, *TBX21 and CCL4*) enriched

in human cluster CD4T_7 (red boxes). **b**, Feature plot showing expression of *FOXP3* gene (blue dots) in the human $CD4^+$ T single-cell dataset. T_{reg} cell cluster CD4T_17, previously identified as T_{reg} cells, highlighted. **c**, Frequencies of cells that expressed each of the exT_{reg} cell signature genes in CD4T_7 (red circles) and CD4T_17 (T_{reg} cells, blue circles). n = 61. **d**, Cells expressing optimal exT_{reg} cell candidate gene combination (*CST7* + *NKG7* + *GZMA* + *PRF1* + *TBX21*) are highlighted in red on UMAP embeddings of $CD4^+$ T clusters from the scRNA-seq data. All other cells are in gray. **e**, Differentially expressed surface markers (CITE-seq antibodies) on cells expressing candidate gene combinations. Average log_2FC (dot color) and log_2(pct.1/pct.$_2$) × avg_log_2FC (dot size) for significant (P < 0.05) differentially expressed protein markers on candidate cells versus CD4T_17 (T_{reg} cells) are shown. Enriched exT_{reg} markers CD127, CD16 and CD56 are marked with red boxes. The second-to-last combination is candidate 5 (*CST7* + *NKG7* + *GZMA* + *PRF1* + *TBX21*). **f**, UMAP embeddings of $CD4^+$ T clusters. Black outline marks cluster CD4T_7; cells that coexpressed CD16 and CD56 are shown as red dots. **g**, Representative plots from flow cytometry (FACS) showing $CD16^+CD56^+CD4^+$T cells (exT_{reg} cells, red) and $CD25^+CD127^{lo}CD4^+$T cells (T_{reg} cells, blue) with FMO controls. **h**, MFI of CD16 (n = 6), CD56 (n = 6), CD127 (n = 3) and FOXP3 (n = 6) expression in exT_{reg} cells (red circles) and T_{reg} cells (blue circles). 20% male, 80% female donors; ages 23–64 years. Results (**c** and **h**) are represented as the mean ± s.e.m. Each dot (**c** and **h**) represents a biological replicate from an independent human donor. Statistical comparisons using a two-tailed Mann–Whitney U test (**c** and **h**) and a two-tailed Wilcoxon's rank-sum test with Benjamini–Hochberg correction for multiple comparisons (**a** and **e**). In **c**, ****P < 0.000000000000001 for *CST7*, *NKG7*, *GZMA*, *PRF1* and ****$P = 3.86 \times 10^{-13}$ for *TBX21*. In **h**, *P = 0.0121, **P = 0.0022.

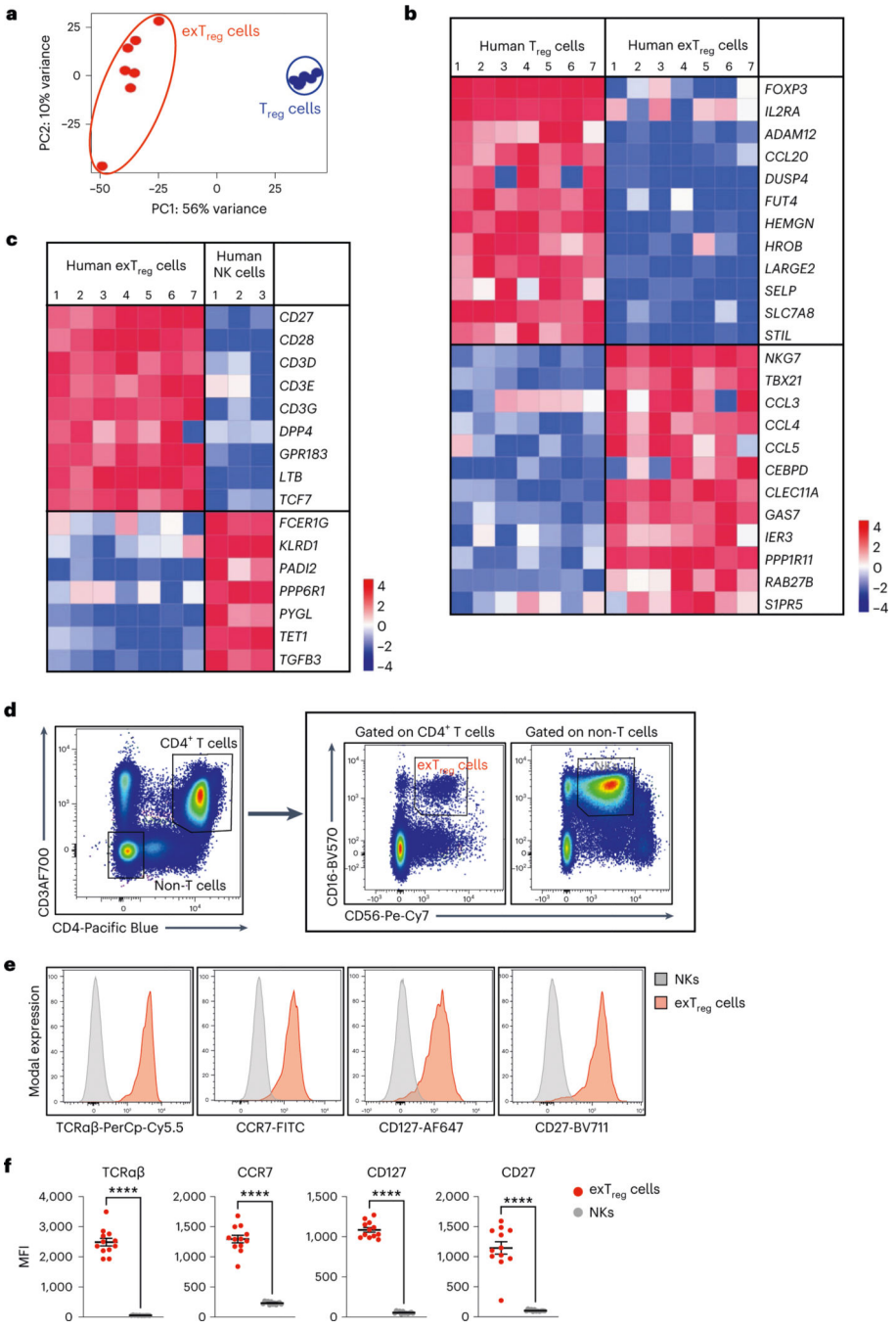

Fig. 3 |. Deep transcriptomes from sorted human $CD3^+CD4^+CD16^+CD56^+$ exT_{reg} cells contrasted with T_{reg} cells and NK cells.

a, PCA plot of bulk RNA-seq data from sorted human exT_{reg} ($CD3^+CD4^+CD16^+CD56^+$) and T_{reg} ($CD3^+CD4^+CD25^+CD127^{lo}$) cells. $n = 7$. Donor details for human bulk RNA-seq in Supplementary Table 13. **b**,**c**, Comparative gene signature analysis between human exT_{reg} cells and T_{reg} cells (**b**) or NK (**c**) cells. Genes were filtered for significant differential expression, consistent in both mouse and human datasets (only human shown here). An external dataset was used for human NK cells: GSE133383 (samples GSM3907331,

GSM3907341 and GSM3907351). Lowly expressed genes (<7 raw reads in all samples) in our dataset were filtered out. EdgeR was used to normalize the counts by applying the trimmed mean of M-values method and counts-per-million conversion. Analysis of DEGs was done using DESeq2. Curated lists of significant DEGs ($log_2FC \pm 1$, adjusted $P < 0.05$) genes are shown on normalized heat maps, scaled by row (z scores). **d**, Representative FACS plots showing exT_{reg} cells as $CD3^+CD4^+CD16^+CD56^+$ T cells and NK cells as $CD3^-CD4^-CD16^+CD56^+$ non-T cells in hPBMCs. **e**, Histograms showing the fluorescence intensities of conjugated antibodies against TCRαβ, CCR7, CD127 and CD27 on NK cells (gray) and exT_{reg} cells (red). The scaled y axis was normalized to mode. **f**, MFI values of the specified markers ($n = 12$ for each) in NK cells (gray circles) and exT_{reg} cells (red circles) were plotted as the mean ± s.e.m. 40% male and 60% female donors, aged 20–69 years. Each dot represents a biological replicate from an independent human donor. Statistical comparisons were done using a two-tailed Wald test with Benjamini–Hochberg correction for multiple testing (**b** and **c**) and a two-tailed Mann–Whitney U test (**f**). **** $P = 7.396 \times 10^{-7}$ in **f**.

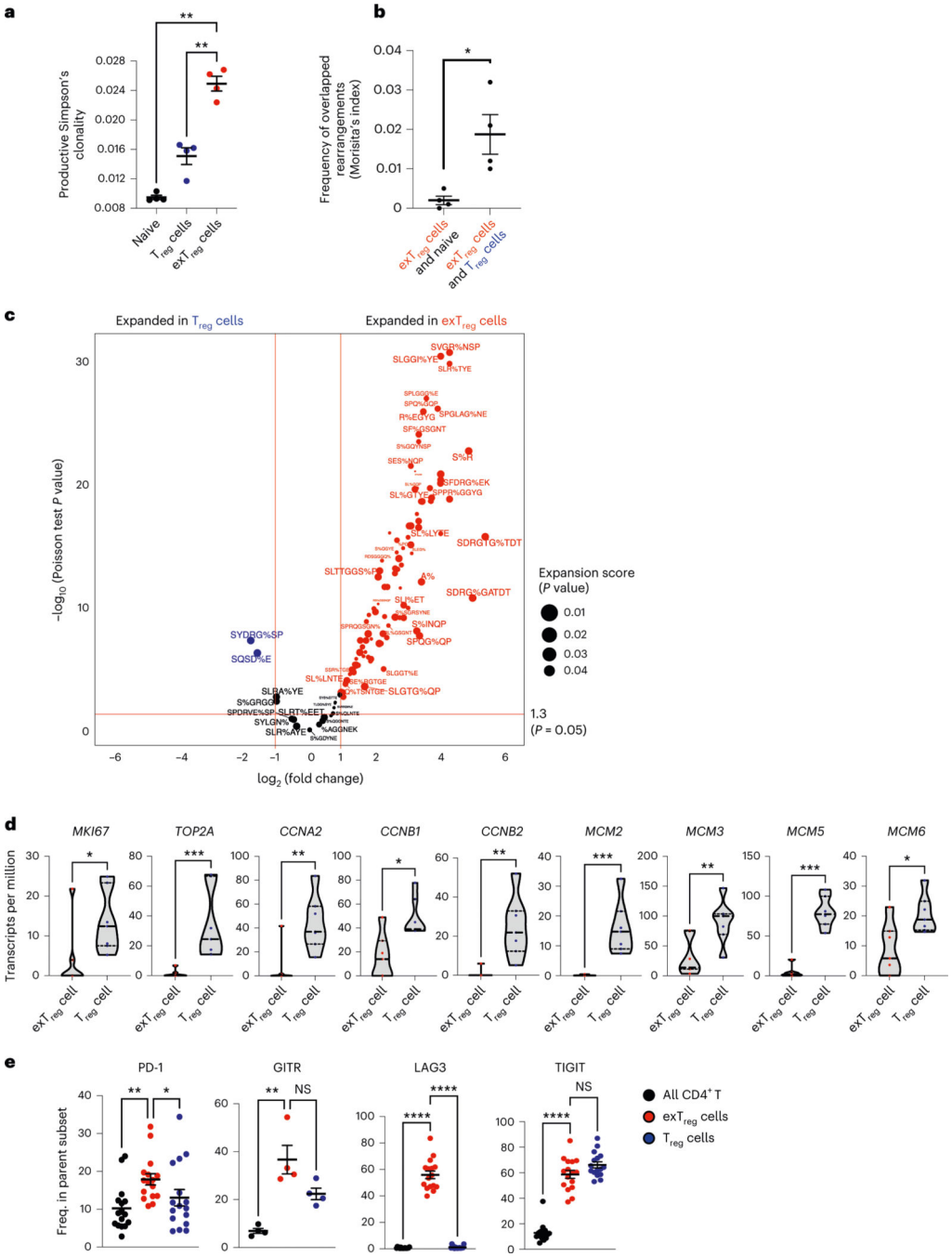

Fig. 4 |. Oligoclonal human exT$_{reg}$ cells are clonally expanded from proliferating T$_{reg}$ cells.
a, Productive Simpson's clonality of TCRβ sequences from sorted naïve T cells (black circles), T$_{reg}$ cells (blue circles) and exT$_{reg}$ cells (red circles). $n = 4$. Donor details for human TCR-seq in Supplementary Table 13. **b**, Frequency of rearrangements shared between exT$_{reg}$ cells and naïve or between exT$_{reg}$ cells and T$_{reg}$ cells was measured using Morisita's index. $n = 4$. Results (**a** and **b**) are represented as the mean ± s.e.m. **c**, GLIPH2-analyzed conserved amino acid motifs in TCRβ sequences. Groups with exT$_{reg}$ TCRs were filtered for statistically significant expansion score ($P < 0.05$). 178 of 345 expanded exT$_{reg}$ GLIPH2

groups were shared by T_{reg} cells. Relative abundance of T_{reg} and exT_{reg} TCRs in these 178 T_{reg}/exT_{reg} groups was compared and DEG patterns ($log_2FC \pm 1$, two-sided Poisson test $P < 0.05$) are shown as a volcano plot. Horizontal line at $-log_{10}$ (P value) = 1.3 (same as $P = 0.05$). Vertical lines at $|log_2FC| = 1$. **d**, Violin plots showing normalized expression levels (transcripts per million) of proliferation genes *MKI67*, *TOP2A*, *CCNA2*, *CCNB1*, *CCNB2*, *MCM2*, *MCM3*, *MCM5* and *MCM6* in human bulk transcriptomes from sorted human T_{reg} cells (blue dots) and exT_{reg} cells (red dots). $n = 7$. 33.33% male and 66.67% female donors, aged 21–54 years. **e**, Frequency of PD-1 ($n = 16$), GITR ($n = 4$), LAG3 ($n = 16$) and TIGIT ($n = 16$) expressing cells by FACS, percentage of parent (all $CD4^+$T cells (black circles), exT_{reg} cells (red circles), T_{reg} cells (blue circles); mean ± s.e.m.). 50% male and 50% female donors, aged 20–69 years. Each dot represents a biological replicate from an independent donor. Statistical comparisons were done using one-way analysis of variance (ANOVA) with Dunnett's multiple-comparison test (**a**), a two-tailed Mann–Whitney U test (**b** and **d**) and a Kruskal–Wallis test, adjusted with Dunn's multiple-comparison testing (**e**). In **a**, exT_{reg} cells versus naive $^{**}P = 0.0012$; versus T_{reg} cells $^{**}P = 0.0068$. In **b**, $^{*}P = 0.0286$. In **d**, $^{*}P = 0.0111$ for *MKI67*, *CCNB1*; $^{*}P = 0.0175$ for *MCM6*; $^{**}P = 0.007$ for *CCNA2* and *MCM3*; $^{**}P = 0.0012$ for *CCNB2*; $^{***}P = 0.0006$ for *TOP2A*, *MCM2*, *MCM5*. In **e**, PD-1 $^{**}P = 0.0023$, GITR $^{**}P = 0.0047$, LAG3 $^{****}P = 3.21 \times 10^{-7}$, TIGIT $^{****}P = 5.227 \times 10^{-5}$ for exT_{reg} cells versus $CD4^+$T cells; PD-1 $^{*}P = 0.0329$, GITR $P = 0.3396$, LAG3 $^{****}P = 1.659 \times 10^{-5}$, TIGIT $P = 0.423$ for exT_{reg} cells versus T_{reg} cells. NS, not significant.

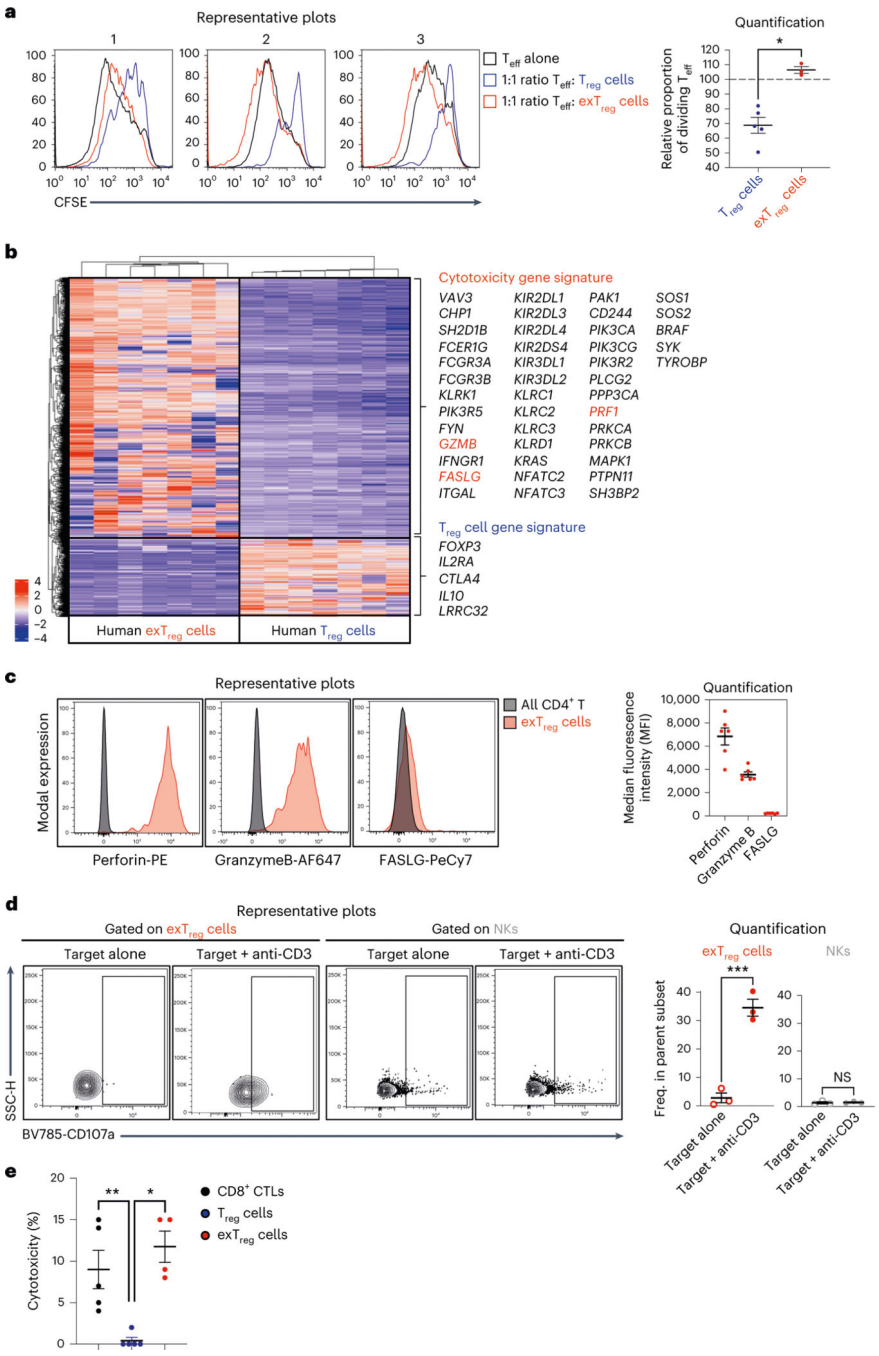

Fig. 5 |. Human exT$_{reg}$ cells are not suppressive but are cytotoxic.

a, CFSE-labeled CD3^{+}CD4^{+}CD25^{-}T cells (T$_{eff}$) were co-cultured at 1:1 ratio with either CTV-labeled T$_{reg}$ cells or exT$_{reg}$ cells, in the presence of anti-CD3/CD28/CD2-coated beads. Left, representative histograms from three independent experiments showing CFSE in T$_{eff}$ cells alone (black line), in T$_{eff}$ cells cultured with T$_{reg}$ cells (blue line) and in T$_{eff}$ cells cultured with exT$_{reg}$ cells (red line). Right, proportion of dividing T$_{eff}$ cells after 5 d of co-culture with T$_{reg}$ cells (blue circles, $n = 5$) or ex T$_{reg}$ cells (red circles, $n = 3$). 40% male and 60% female donors; aged 23–43 years. **b**, Heat map of DEGs ($P < 0.01$ and $|\log_2 FC| >$

2, based on a two-tailed Wald test with Benjamini–Hochberg *P*-value adjustment) between human exT_{reg} versus T_{reg} transcriptomes from Fig. 3. Cytotoxic and T_{reg} signature genes are highlighted. **c**, FACS analysis of cytotoxic proteins FASLG, perforin and granzyme B (genes are labeled red in **b**) in human exT_{reg} cells, compared to bulk $CD4^+$T cells. Left, representative histograms of intensities of fluorochrome-conjugated antibodies against FASLG, perforin and granzyme B on exT_{reg} cells (red) and all $CD4^+$T cells (black). Right, MFIs of marker protein expression in exT_{reg} cells. $n = 6$. 50% male and 50% female donors, aged 25–37 years. **d**, Representative contour plots (left) and quantification (right) of basal and anti-CD3-induced degranulation in exT_{reg} cells (red) and NK cells (gray), as measured by surface mobilization of the degranulation marker CD107a by FACS. hPBMCs were co-cultured with uncoated P815 cells (target alone, open circles) or 5 μg ml^{-1} anti-CD3-coated P815 cells (target + anti-CD3, filled circles) for 6 h at a 10:1 PBMC:P815 ratio. $n = 3$. 33.33% male and 66.67% female donors; aged 25–38 years. **e**, Anti-CD3-loaded P815 cells were co-cultured with CD8 CTLs (black circles, $n = 5$), T_{reg} cells (blue circles, $n = 5$) or exT_{reg} cells (red circles, $n = 4$) at a 1:5 P815:effector cells ratio for 16 h. 60% male and 40% female donors, aged 21–45 years. Cytotoxicity was assessed by measuring lactate dehydrogenase amounts in the supernatant. Results (**a** and **c**–**e**) are represented as the mean ± s.e.m. Each dot represents a biological replicate from an independent donor. Statistical comparisons were done using a two-tailed Mann–Whitney *U* test (**a** and **e**) and a two-tailed unpaired *t*-test (**d**). $*P = 0.0357$ (**a**). $***P = 0.0008$ (**d**, exT_{reg} cells); $P = 0.7707$ (**d**; NKs). $**P = 0.0079$ (**e**, T_{reg} cells versus CTLs); $*P = 0.0159$ (**e**; T_{reg} cells versus exT_{reg} cells).

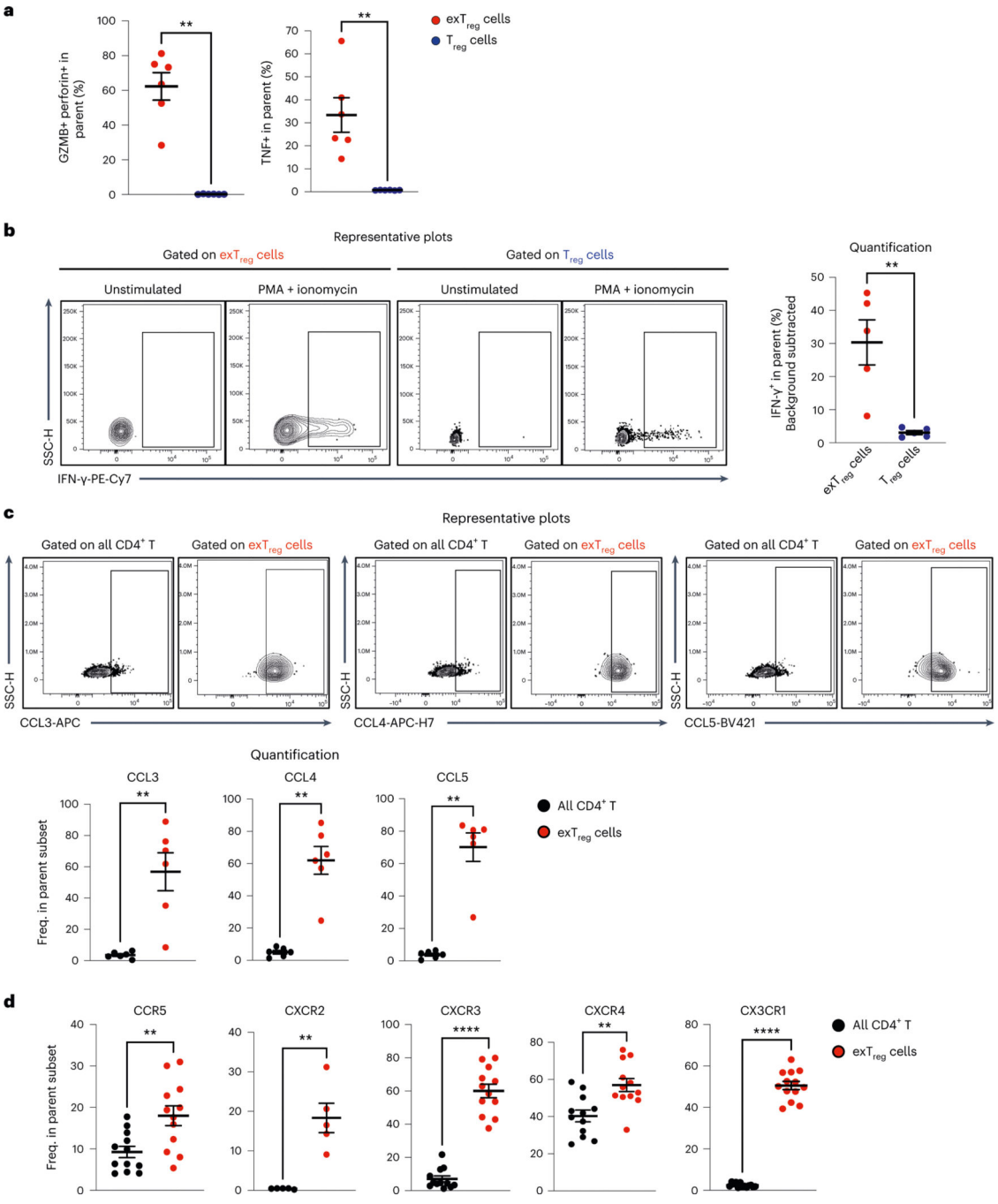

Fig. 6 |. Human exT$_{reg}$ cells express cytotoxic proteins, inflammatory cytokines, chemokines and chemokine receptors.

a, Frequencies of GzmB$^+$perforin$^+$ and TNF$^+$ cells in T$_{reg}$ cells (blue circles) and exT$_{reg}$ cells (red circles) were assessed in an ICS assay by FACS. *n* = 6. 50% male and 50% female donors; aged 24–39 years. **b**, Representative contour plots (left) showing intracellular expression of IFN-γ under unstimulated and PMA–ionomycin-stimulated conditions in exT$_{reg}$ cells and T$_{reg}$ cells. Right, frequency of PMA-induced IFN-γ in exT$_{reg}$ cells (red circles) and T$_{reg}$ cells (blue circles). *n* = 5. 40% male and 60% female donors; aged

23–39 years. **c**, hPBMCs were stained for intracellular expression of CCL3 (MIP-1α), CCL4 (MIP-1β) and CCL5 (RANTES). Top, representative contour FACS plots showing expression among all $CD4^+$T cells and in exT_{reg} cells. Bottom, frequencies of $CCL3^+$, $CCL4^+$ and $CCL5^+$ cells among the parent subset (all $CD4^+$T cells (black circles), exT_{reg} cells (red circles)). $n = 6$. 50% male and 50% female donors, aged 26–33 years. **d**, Frequencies of CCR5 ($n = 12$), CXCR2 ($n = 5$), CXCR3 ($n = 12$), CXCR4 ($n = 12$) and CX3CR1 ($n = 13$) chemokine receptor-expressing exT_{reg} cells (red circles) and all $CD4^+$T cells (black circles). 40% male and 60% female donors, aged 20–69 years. Results (**a**–**d**) were plotted as the mean ± s.e.m. Each dot represents a biological replicate from an independent donor. Statistical comparisons were performed using a two-tailed Mann–Whitney *U* test (**a**–**d**). $^{**}P = 0.0022$ (**a**), $^{**}P = 0.0079$ (**b**), $^{**}P = 0.0022$ (**c**). In **d**, $^{**}P = 0.0068$ (CCR5), $^{**}P = 0.0079$ (CXCR2), $^{****}P = 7.396 \times 10^{-7}$ (CXCR3), $^{**}P = 0.0023$ (CXCR4), $^{****}P = 1.92 \times 10^{-7}$ (CX3CR1).

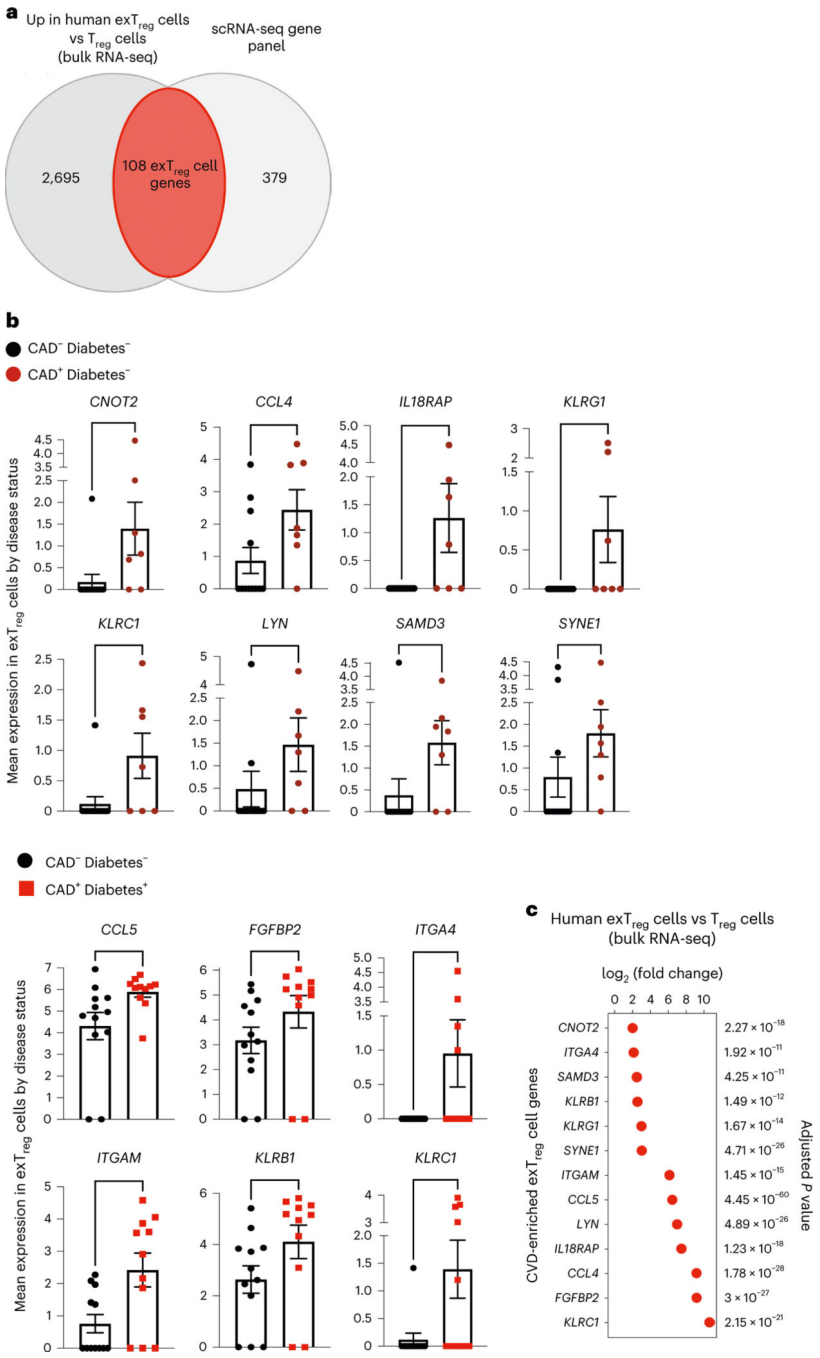

Fig. 7 |. Inflammatory and cytotoxic human exT$_{reg}$ genes overexpressed in individuals with coronary artery disease.

a, Genes that were significantly upregulated in human exT$_{reg}$ cells compared to T$_{reg}$ cells (2,803 genes) in the human bulk RNA-seq data (Fig. 3) were intersected with the genes present in the published human scRNA-seq panel (Fig. 2). Donor details for human bulk RNA-seq are in Supplementary Table 13 and those for scRNA-seq are in ref. 21. **b**, Mean expression of genes in CD16$^+$CD56$^+$ exT$_{reg}$ cells from the scRNA-seq dataset that were significantly increased in CAD$^+$ non-diabetic (brown circles in top, $n = 7$) or diabetic (red

squares in bottom, $n = 11$) individuals in comparison to control CAD^- non-diabetic (black circles, $n = 12$) individuals. Results are shown as the mean ± s.e.m. Each point represents data from exT_{reg} cells from an independent donor. Statistical comparisons were done using a two-tailed Mann–Whitney *U* test. Top, $^{**}P = 0.0064$ (*CNOT2*), $^{*}P = 0.0414$ (*CCL4*), $^{**}P = 0.009$ (*IL18RAP*), $^{*}P = 0.0361$ (*KLRG1*), $^{*}P = 0.0163$ (*KLRC1*), $^{*}P = 0.0371$ (*LYN*), $^{**}P = 0.0095$ (*SAMD3*), $^{*}P = 0.0395$ (*SYNE1*). Bottom, $^{*}P = 0.0126$ (*CCL5*), $^{*}P = 0.0354$ (*FGFBP2*), $^{*}P = 0.0373$ (*ITGA4*), $^{*}P = 0.018$ (*ITGAM*), $^{*}P = 0.031$ (*KLRB1*), $^{*}P = 0.032$ (*KLRC1*). **c**, log_2FC and adjusted *P* values of a DEG analysis (based on a two-tailed Wald test with Benjamini–Hochberg *P*-value adjustment) between exT_{reg} cells and T_{reg} cells for the 13 CAD-relevant exT_{reg} genes from **b**.